Journal of Metallurgy

Thermal and Mechanical Treatments of Al, Al Alloys, and Other Lightweight Metals and Alloys

Guest Editors: Enrico Evangelista, Michael E. Kassner, and Chong Soo Lee

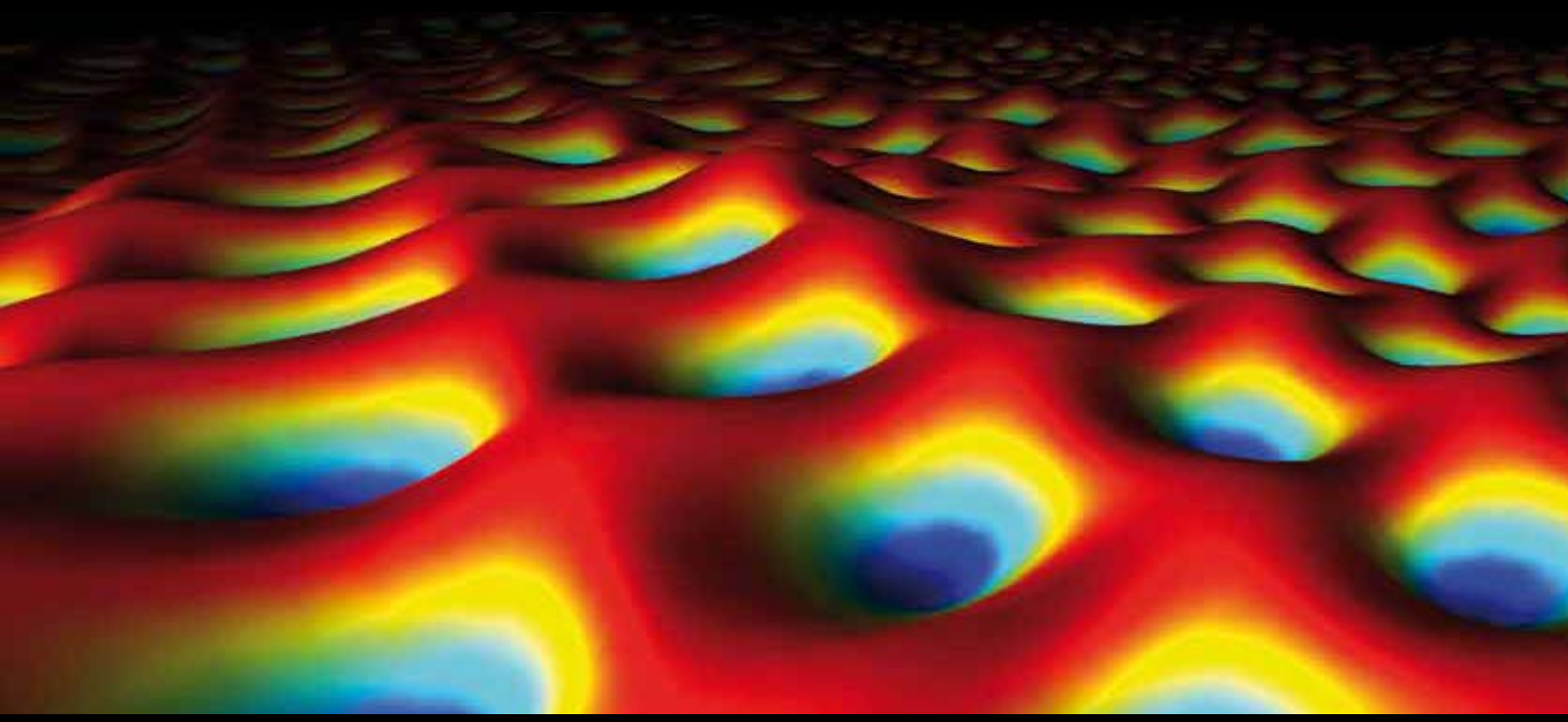

Thermal and Mechanical Treatments of Al, Al Alloys, and Other Lightweight Metals and Alloys

Journal of Metallurgy

Thermal and Mechanical Treatments of Al, Al Alloys, and Other Lightweight Metals and Alloys

Guest Editors: Enrico Evangelista, Michael E. Kassner, and Chong Soo Lee

Editorial Board

Contents

Hindawi Publishing Corporation
Journal of Metallurgy
Volume 2012, Article ID 294874, 2 pages
doi:10.1155/2012/294874

Editorial

Thermal and Mechanical Treatments of Al, Al Alloys, and Other Lightweight Metals and Alloys

Hugh J. McQueen,[1] Enrico Evangelista,[2] Michael E. Kassner,[3] and Chong Soo Lee[4]

[1] *Materials Processing Mechanical/Industrial Engineering, Concordia University Montreal, QC, Canada H3G 1M8*
[2] *Department of Metallurgy, Polytechnic University, I 60131 Ancona, Italy*
[3] *Office of Naval Research, Arlington, VA 22203, USA*
[4] *Graduate Institute of Ferrous Technology, Pohang University of Science and Technology, Pohang 790-784, Republic of Korea*

Correspondence should be addressed to E. Evangelista, enricoevangelista@tiscali.it

Received 9 May 2012; Accepted 9 May 2012

Thermomechanical processing was first coined for steels in the 1950s, but it had been around since the 1850s, when Kirkaldy conducted extensive research linking processing, tensile properties, and microstructures, including fractographs [1–3]. Often, it was practiced without complete understanding, as for eutectoid steel in rolling and cooling and in patenting wire with transformation and wire drawing [4]. For Al, improved processing schedules were found for Al-Mg-Si alloys in press quenching after hot extrusion and in solution treating before cold impact extrusion [5–10]. The wide variety of TMP for Al is found in a recent book [11] that relates it to all classes of alloys and to rolling [12–16], extrusion [8, 9, 16], and forging [17]. TMP has spread to many metals as noted in the adjoining papers developed to level that modeling is possible [18].

In broad definition, TMP is a sequence of temperature and strain operations to produce a shape and a microstructure with outstanding properties for that alloy [19, 20]. If a step obliterates the previous microstructures, then the whole sequence does not qualify as TMP [7, 10, 11, 16]. Time or space breaks are permitted, for example, multistage cold rolling to suitable strain, annealing to a fine grain size and finally deep drawing or preaging an Al autobody panel so that precipitation is completed in the paint baking process [21]. The processing becomes more valuable if several steps can be combined, thus saving in labor, equipment, and energy [7–9, 16]. Preliminary research must be conducted to understand the effects of ranges in composition, temperature, and strain rate, as exemplified in the papers that follow.

Al and Mg alloys have no allotropic transformations but can be precipitation hardened. Generally, Al can be worked over the range of 200–500°C [19, 20, 22–24], whereas Mg has insufficient operating slip systems below 200°C and above that has less uniform substructures and lower ductility than comparable Al alloys [25]. Dislocation substructures vary by temperature and strain rate have significant effects on particle distributions [10, 11, 24] and in superplastic behavior [6, 26]. The paper by M. E. Kassner et al. compares quench sensitivity of two Al-Mg-Si alloys, and Fare et al. consider the effect of severe deformation on aging. The influence of temperature on an Mg alloy is reported by Yeom et al.

Steels and Ti alloys have an allotropic transformation [3, 27, 28] that develops a variety microstructures dependent on composition and cooling rate usually with different precipitation behaviors for the same alloying [1, 3, 4, 29, 30]. Structural refinement can be enhanced in the course of shaping by changing from one phase to another or by manipulating the duplex structure [3, 31, 32]. Steels have by far the widest selection of TMP, such as controlled rolling for ferrite grain refining and carry-over of substructures into bainite or martensite to name a few; each of these with many options depends on the solute or precipitation alloying [1, 18, 29, 33]. Dislocation substructures play a significant role in nucleation of the new phase or are carried through a martensitic type, as well as nucleating particles [30, 31, 34]. Fundamental aspects of these possibilities are clarified in

the papers by Yeom et al. (extrusion Ti 6 Al-4V) and by Li et al. (martensite Ti-3.5Al-4.5Mo).

H. J. McQueen
E. Evangelista
M. Kassner
C. S. Lee

References

[1] H. J. McQueen, "Historical aspects of thermomechanical processing for steels," *Materials Science Forum*, vol. 539–543, no. 5, pp. 4397–4404, 2007.

[2] H. J. McQueen, "Successful transition from wrought iron to steel in hot work processing with mechanism differences," *Materials Science Forum*, vol. 638-642, pp. 3380–3387, 2010.

[3] C. M. Sellars, "Hot working and forming processes," C. M. Sellars and G. J. Davies, Eds., pp. 3–15, Metals Society, London, UK, 1980.

[4] H. J. McQueen, "Behavior of pearlite in thermomechanical processing and service-historical perspective," *Materials Science Forum*, vol. 706-709, pp. 2776–2781, 2012.

[5] C. M. Sellars, "Al alloys, physical mechanical properties," in *Proceedings of the International Conference on Aluminium Alloys (ICAA3 '92)*, L. Arnberg et al., Ed., vol. 3, pp. 89–105, NTH/SINTEFF, Trondheim, Norway, 1992.

[6] H. J. McQueen and J. J. Jonas, "Therrnomechanical processing (TMP) of aluminum alloys," in *Proceedings of the Aluminium*, C. Q. Chen, Ed., pp. 727–747, Academic Pub, Beijing, China, 1990.

[7] H. J. McQueen, *Materials Science Forum*, vol. 519-523, ICAA10, pp. 1493–1498, 2006.

[8] H. J. McQueen and O. C. Celliers, "Application of hot workability studies to extrusion processing—part II. Microstructural development and extrusion of Al, Al-Mg, and Al-Mg-Mn alloys," *Canadian Metallurgical Quarterly*, vol. 35, no. 4, pp. 305–319, 1996.

[9] H. J. McQueen and O. C. Celliers, "Application of hot workability studies to extrusion processing—part III: physical and mechanical metallurgy of Al-Mg-Si and Al-Zn-Mg alloys," *Canadian Metallurgical Quarterly*, vol. 36, no. 2, pp. 73–86, 1997.

[10] H. J. McQueen and E. Evangelista, "Hot working defines thermomechanical processing (TMP) for aluminum alloys and composites," *Materials Science Forum*, vol. 706–709, pp. 89–96, 2012.

[11] H. J. McQueen, S. Spigarelli, M. E. Kassner, and E. Evangelista, *Hot Deformation and Processing of Aluminum Alloys*, CRC Press (Tailor and Francis Group), Boca Raton, Fla, USA, 2011.

[12] H. J. McQueen, "Substructural influence in the hot rolling of Al alloys," *Journal of the Minerals, Metals and Materials Society*, vol. 50, no. 6, pp. 28–33, 1998.

[13] I. Poschmann and H. J. McQueen, "Static restoration of aluminium during multi-stage hot rolling simulation," *Materials Research and Advanced Techniques*, vol. 87, no. 5, pp. 349–356, 1996.

[14] I. Poschmann and H. J. McQueen, "Multi-step hot working of Al-5 wt.% Mg," *Materials Research and Advanced Techniques*, vol. 88, no. 1, pp. 14–22, 1997.

[15] J. Hirsch, in *Proceedings of the International Conference on Thermomechanical Processing of Steels and Other Materials (Thermec '97)*, T. Chandra and T. Sakai, Eds., pp. 1083–1094, TMS, Warrendale, Pa, USA, 1998.

[16] H. J. McQueen and M. E. Kassner, *Light Weight Alloys for Aerospace Applications*, Edited by K. Jata, TMS-AIME, Warrendale, Pa, USA, 2001.

[17] H. J. McQueen and E. Evangelista, *Materials in the Automotive Industry*, The Metallurgical Society of CIM, Montreal, Canada, 2001.

[18] C. M. Sellars, *From Trial and Error to Computer Modeling of TMP*, Bessemer Lecture, Institute of Metals, Materials, Minerals, London, UK, 2010.

[19] J. G. Morris, Ed., *Thermomechanical Processing of Al Alloys*, Metallurgical Society of AIME, 1979.

[20] E. H. Chia and H. J. McQueen, Eds., *Microstructural Control in Al Alloys*, Metallurgical Society of AIME, Warrendale, Pa, USA, 1986.

[21] D. J. Lloyd, *Advances in Industrial Materials*, Edited by D. S. Wilkinson, The Metallurgical Society of CIM, Montreal, Canada, 1998.

[22] H. J. McQueen, *Hot Deformation of Aluminum Alloys*, TMS-AIME, Warrendale, Pa, USA, 1991.

[23] H. J. McQueen and W. Blum, *Aluminium*, vol. 80, pp. 1151–1159, 2004.

[24] H. J. McQueen, "Aerospace materials and manufacturing IV: advances in processing/repair," in *Proceedings of the 47th Conference of Metallurgists*, M. Jahazi, P. C. Patnaik, and M. Elboudjaini, Eds., pp. 111–123, MetSociety of CIM, Montreal, Canada, 2008.

[25] H. J. McQueen, "Magnesium in the Global Age," M. O. Pekguleryuz and L. W. MacKenzie, Eds., pp. 399–420, MetSociety of CIM, Montreal, Canada, 2006.

[26] B. M. Watts, M. J. Stowell, B. L. Baikie, and D. G. E. Owen, "Superplasticity in Al-Cu-Zr alloys—1. Material preparation and properties," *Metal Science*, vol. 10, no. 6, pp. 189–197, 1976.

[27] D. L. Bourell and H. J. McQueen, "Thermomechanical processing of iron, titanium, and zirconium alloys in the bcc structure," *Journal of Materials Shaping Technology*, vol. 5, pp. 53–73, 1987.

[28] H. J. McQueen and D. L. Bourell, "Hot workability of metals and alloys," *Journal of Metals*, vol. 39, no. 9, pp. 28–35, 1987.

[29] J. J. Jonas and C. M. Sellars, in *Proceedings of the Sir Robert Honeycombe Commemmorative Symppsium*, pp. 147–177, Institute of Materials Royal Society, London, UK, 1992.

[30] H. J. McQueen, N. D. Ryan, and E. V. Konopleva, in *Proceedings of the Guthrie Symposium onMetallurgy*, M. Isac, Ed., pp. 205–211, McGill Metals Processing Center, Montreal, Canada, 2011.

[31] V. M. Khlestov, E. V. Konopleva, and H. J. McQueen, "Effect of deformation in controlled rolling on ferrite nucleation," *Canadian Metallurgical Quarterly*, vol. 40, no. 2, pp. 221–234, 2001.

[32] E. Evangelista, H. J. McQueen, M. Niewczas, and M. Cabibbo, "Hot workability of 2304 and 2205 duplex stainless steels," *Canadian Metallurgical Quarterly*, vol. 43, no. 3, pp. 339–354, 2004.

[33] H. J. McQueen, S. Yue, N. D. Ryan, and E. Fry, "Advanced materials and technologies," L. A. Dobrzanski, Ed., pp. 295–332, Silesian Technical University, Gliwice, Poland, 1995.

[34] H. J. McQueen and E. Evangelista, "Super-high strength steels," A. J. Deardo et al., Ed., Electronic Plenary, p. 22, Associazione Italiana di Metallurgia, Milan, Italy, 2010.

Hindawi Publishing Corporation
Journal of Metallurgy
Volume 2012, Article ID 989834, 6 pages
doi:10.1155/2012/989834

Research Article

Prediction of Microstructure Evolution in Hot Backward Extrusion of Ti-6Al-4V Alloy

Jong-Taek Yeom,[1] Jeoung Han Kim,[1] Jae-Keun Hong,[1] Nho-Kwang Park,[1] and Chong Soo Lee[2]

[1] *Special Alloys Group, Korea Institute of Materials Science, 531 Changwondaero, Changwon 641-831, Republic of Korea*
[2] *Department of Materials Science and Engineering, POSTECH, San 31, Hyojadong, Namgu, Pohang 790-784, Republic of Korea*

Correspondence should be addressed to Jong-Taek Yeom, yjt96@kims.re.kr

Received 28 September 2011; Accepted 21 October 2011

Academic Editor: Enrico Evangelista

Microstructure evolution of Ti-6Al-4V alloy during hot backward extrusion process was simulated with the combined approaches of finite element method (FEM) and microstructure prediction model. From experimental analysis, it can be found that the change of microstructure during hot forming process of titanium alloy has a close relation to α/β phase transformation and grain growth behaviour. A microstructure prediction model was established by considering the change of volume fractions and grain size of both phases varying with process variables and then implemented into the user-defined subroutine of FEM analysis. In order to demonstrate the reliability of the model, the volume fraction and grain size of primary α phase during the hot backward extrusion process of Ti-6Al-4V alloy were simulated. The simulation results were compared with the experimental ones.

1. Introduction

Computer simulation is an important and effective tool for the optimized forming processes and to reduce error which may be caused by trial and error method. Finite element (FE) analysis is widely used for the simulation of shape and microstructure changes in hot forming [1–3]. With the improvement in understanding of the relationship between microstructures and mechanical properties of structural components, the prediction of shape and microstructure changes has become a hot issue in the high-temperature forming.

The high-temperature forming processes for manufacturing titanium alloy products are normally conducted on the equiaxed structure in two-phase ($\alpha + \beta$) field [4]. The microstructure change is mainly indicated as the change of volume fraction and grain size of α and β phases. It may be due to phase transformation and grain growth during the high temperature forming. In the past, most of microstructure simulations have focused on the prediction of the single-phase alloys using the recrystallization and grain growth models [5]. However, only a limited work [6, 7] has been carried out on the simulation for microstructure evolution of Ti-6Al-4V alloy during hot forming processes. Therefore, the aim of this research is to establish the methodology for prediction of the microstructure evolution of Ti-6Al-4V components during high-temperature forming processes, and to develop a useful design tool for obtaining the optimum process condition in the high-temperature forming processes using finite element method (FEM) simulation.

2. Experimental Procedures

The material used in this work was a Ti-6Al-4V alloy billet annealed at 704°C for 2 h with a diameter of 100 mm. The chemical composition of the alloy is 6.32Al, 4.18V, 0.21Fe, 0.014C, 0.18O, 0.008N, 0.001Y, and balance Ti (in wt%). Initial microstructure of Ti-6Al-4V alloy was an equiaxed structure with the primary α grain size of about 16 μm as shown in Figure 1.

In order to investigate flow behavior and microstructure evolution of Ti-6Al-4V alloy in the α-β phase field,

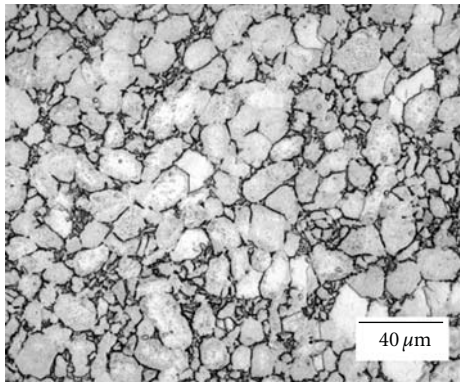

Figure 1: Typical microstructure of the annealed Ti-6Al-4V alloy billet.

compression and heat treatment tests were carried out. Compression tests were performed in the temperature ranges between 850°C and 1000°C with 25°C intervals using the strain rate ranging from 10^{-3} to $10\,s^{-1}$. Heat treatment tests were carried out with the holding time of 30 min between 900 and 1015°C. To observe the actual microstructure at the test temperature, after the holding time of 30 min, the heat-treated samples were water-quenched. To analyze the microstructure evolution during cooling, the samples were heat-treated at the temperature of 900, 925, 950, and 975°C for 30 min. Following the heat treatment, the samples were cooled down using different cooling rates.

In order to verify the reliability of the established microstructure prediction model, Ti-6Al-4V alloy tube was manufactured by hot backward extrusion process using a 150 ton hydraulic press. Backward extrusion process for evaluating the reliability of the model was selected to predict microstructure variation during actual hot working considering friction, interface heat transfer, and process variables. The design of the dies (punch and lower die) and preform is represented in Figure 2. Oil-based graphite lubricant was spread into the punch and lower dies to reduce die friction. The preform of Ti-6Al-4V alloy was glass-coated and heated to an extrusion temperature of 970°C. The punch and die temperatures were selected at 500°C and 600°C, respectively. After the backward extrusion, the Ti-6Al-4V tube was water-quenched.

3. Results and Discussion

Figure 3 shows the change of microstructures with increasing the heating temperature obtained from isothermal heat treatment tests of Ti-6Al-4V alloy. It can be found that the volume fraction and grain size of α phase decrease with increasing the heating temperature, and especially the grain size of α phase markedly decreases from more than 950°C. The β phase grains remain constant up to 950°C and dramatically grow at 975°C. This is in agreement with the observations by Semiatin et al. [8].

Figure 4 shows the change of microstructure with increasing hold time obtained from isothermal heat treatment tests of Ti-6Al-4V alloy. It is noted that the α grain

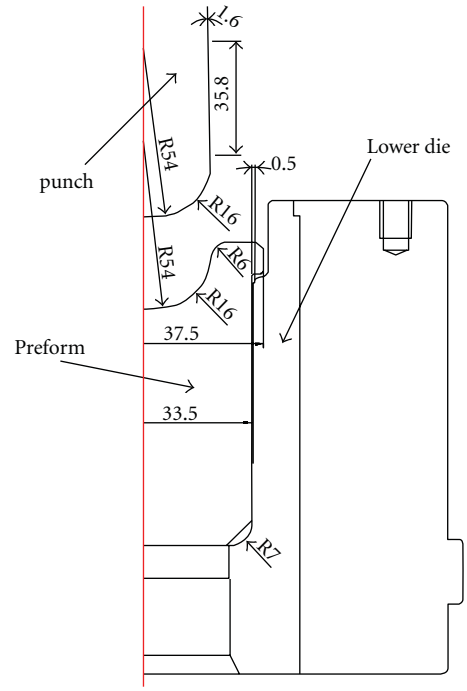

Figure 2: Design of the punch, lower die, and preform used in hot backward extrusion.

size does not change significantly with holding time whereas β grain size increases considerably. This is due to the high diffusivity in β phase.

In general, mechanical properties of Ti-6Al-4V alloy products forged at α-β region were directly affected by the volume fraction and grain size of equiaxed primary α phase. The microstructure prediction model reflecting microstructure evolution during heating and high temperature deformation is established in this work. To predict the volume fraction and grain size of primary α phase, the geometrical model for grain size change of α phase developed in previous work [2, 9, 10] was used. Assuming that the total numbers of α grains and β grain size are constant, the grain size of α phase (d) can be calculated by following equation:

$$d = d_0 \left(\frac{f_\alpha}{f_{\alpha 0}} \right)^{1/3} \quad (\mu\text{m}), \tag{1}$$

where d_0 and $f_{\alpha 0}$ are the initial grain size and volume fraction of primary α phase, respectively, and f_α is the present volume fraction of primary α phase. Meanwhile, the volume fractions of each phase during heating and soaking can be expressed as a function of initial volume fractions of each phase and temperature

$$\begin{aligned} f_\alpha &= f_{\alpha,RT} + \left(1 - \exp\left(-k \cdot \left\langle T_\beta - T \right\rangle\right)\right) \\ f_\beta &= 1 - f_\alpha, \end{aligned} \tag{2}$$

where f_{β_0} and f_β are initial volume fraction and present volume fraction of β phase, respectively. $f_{\alpha,RT}$ is the volume fraction of primary α phase at room temperature. The magnitude of $\langle T_\beta - T \rangle$ is zero when $T_\beta - T \leq 0$, and it is

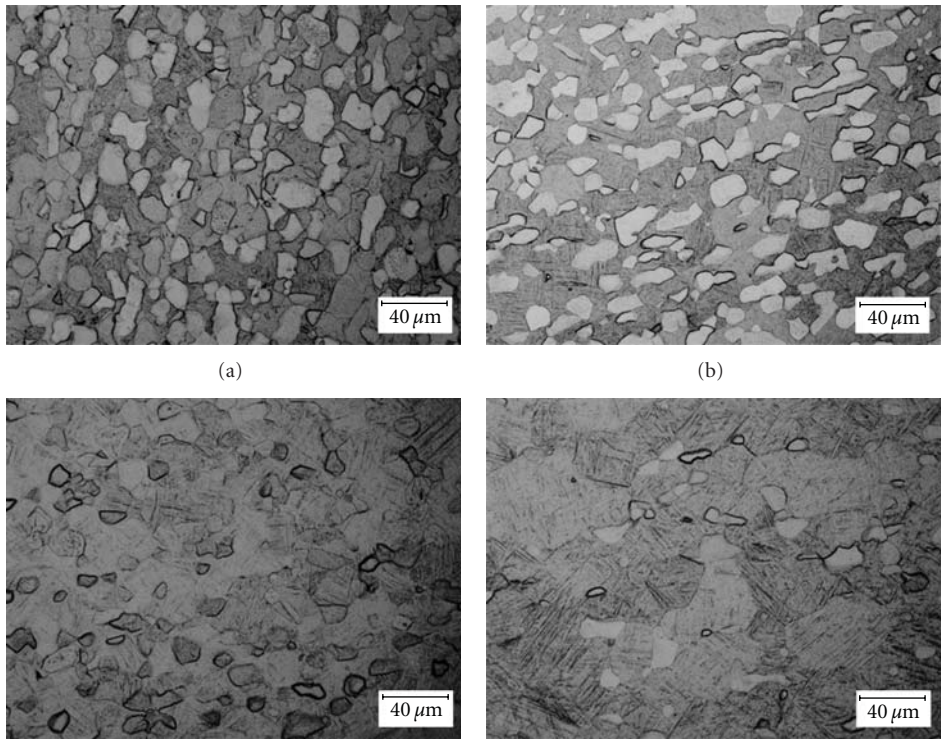

Figure 3: Microstructures of Ti-6Al-4V alloy samples water quenched after a 30 min heat treatment at (a) 900°C, (b) 925°C, (c) 950°C, and (d) 975°C.

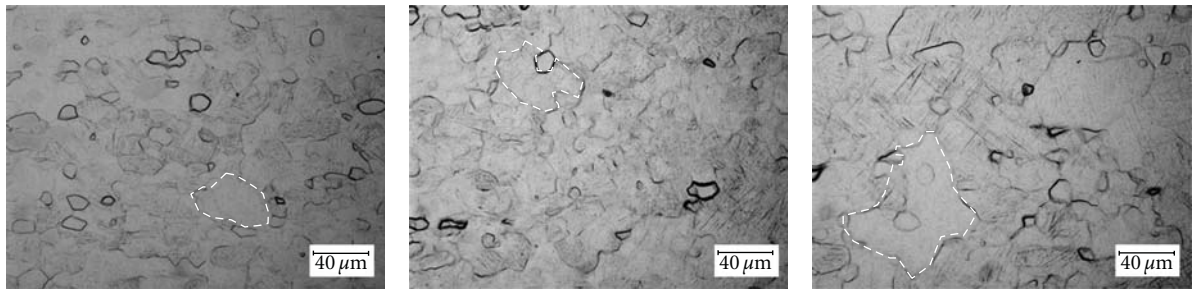

Figure 4: Microstructures of Ti-6Al-4V alloy samples water quenched after isothermal heat treatment at 950°C for (a) 10 min, (b) 1 h, and (c) 10 h. White dotted lines indicate β grains.

$T_\beta - T$ in other case. Through the isothermal heat treatment tests, the parameters $f_{\alpha,RT}$ and k in Ti-6Al-4V alloy with an equiaxed structure were determined by 0.942 and 8.17×10^{-3}, respectively.

In α-β Ti alloys, phase transformation ($\beta \rightarrow \alpha$) also occurs during cooling and forming. In order to express the volume fraction change of α phase during cooling and forming, the Avrami-type equation was applied

$$f_{\alpha,c} = f_{\alpha,h} + \left(f_{\alpha,RT} - f_{\alpha,h}\right) \cdot \left(1 - \exp\left(-f(T) \cdot t^n\right)\right)$$
$$f(T) = A \cdot \left(\frac{T_{\text{heat}} - T}{T_{\text{heat}} - T_e}\right)^{n'}, \tag{3}$$

where $f_{\alpha,h}$ are the volume fraction of α phase after heating and soaking. T_{heat} is heating or soaking temperature. T_e represents the finishing temperature of phase transformation and this value is assumed to be 298 K. The values of n, n', and A were 1, 6.67, and 0.0023, respectively.

A commercial FEM code, DEFORM 2D, was used to simulate the effect of process variables in hot backward extrusion process of Ti-6Al-4V alloy on the distribution of the internal state variables such as strain, strain rate, and temperature. The flow stress data obtained from compression tests were corrected for temperature increment calculated by the following equation:

$$\Delta T = \frac{0.9 \int_0^{\varepsilon} p\sigma d\varepsilon}{\rho C}, \tag{4}$$

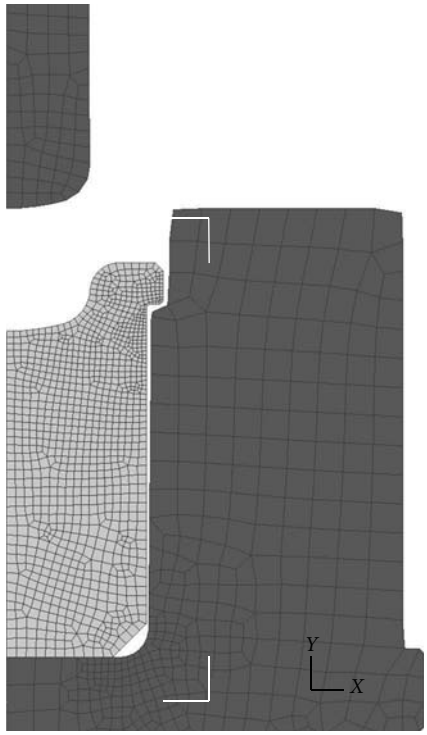

Figure 5: FEM modeling for hot backward extrusion process of Ti-6Al-4V alloy.

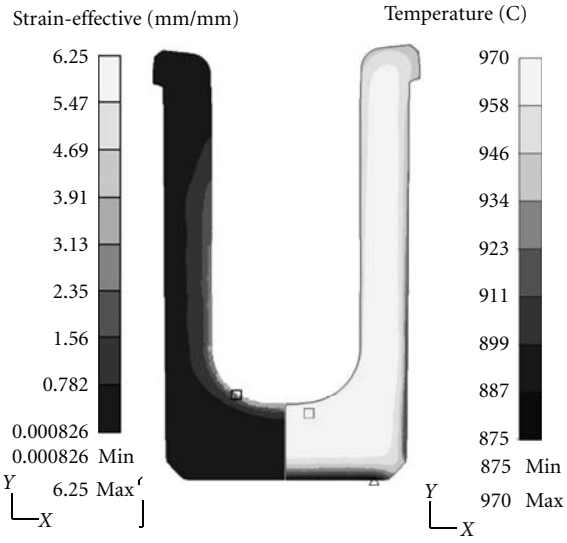

Figure 6: Temperature and effective strain contours for hot backward extrusion simulation of Ti-6Al-4V alloy.

where ε_p is plastic strain, ρ is density of material, and C is specific heat. Corrected flow stress data were directly used to simulate material behavior of Ti-6Al-4V alloy during hot backward extrusion.

Generally, the friction between dies and workpiece is expressed by the friction law of constant factor. Also, interface heat transfer between dies and workpiece greatly affects the temperature change of the workpiece during hot forming process. Based on the results of previous work [11], the friction coefficient and interface heat transfer coefficient were determined at 0.3 and 5.0 kW/m$^{2\circ}$C, respectively. The element used in the simulation is brick elements, and automatic remeshing system was adopted during simulation. Figure 5 shows the 2D modeling for dies and initial preform shapes.

Figure 6 shows simulation results of strain and temperature distributions of hot backward extrusion process of Ti-6Al-4V alloy tube. The simulation results indicate that the highest strain region in the workpiece is found at inner wall, which is in contact with the punch during

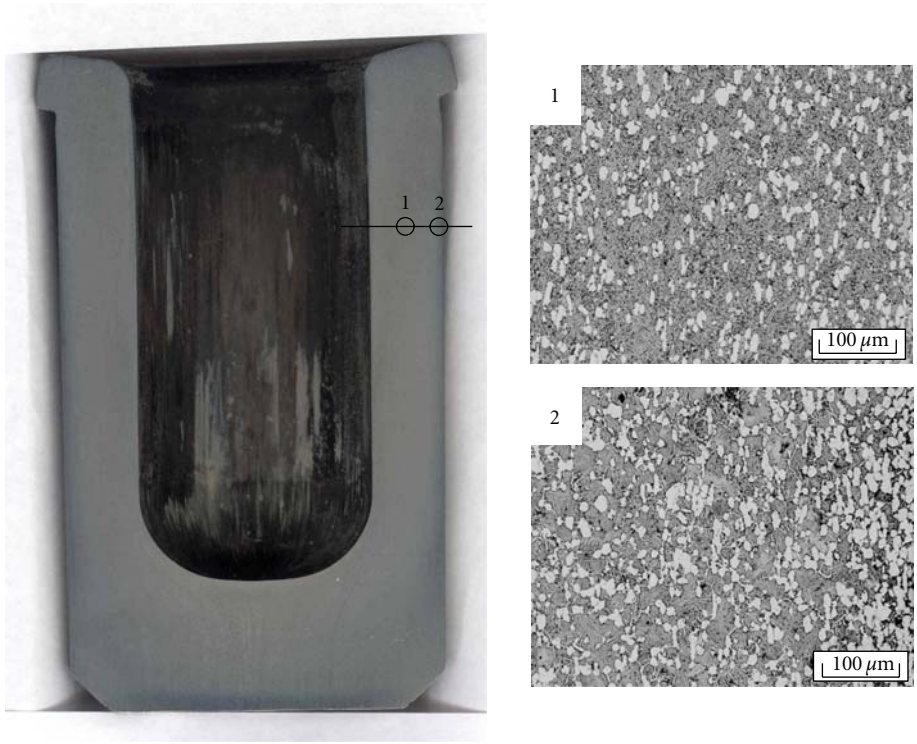

Figure 7: Microstructures observed at different locations for backward extruded Ti-6Al-4V alloy tube.

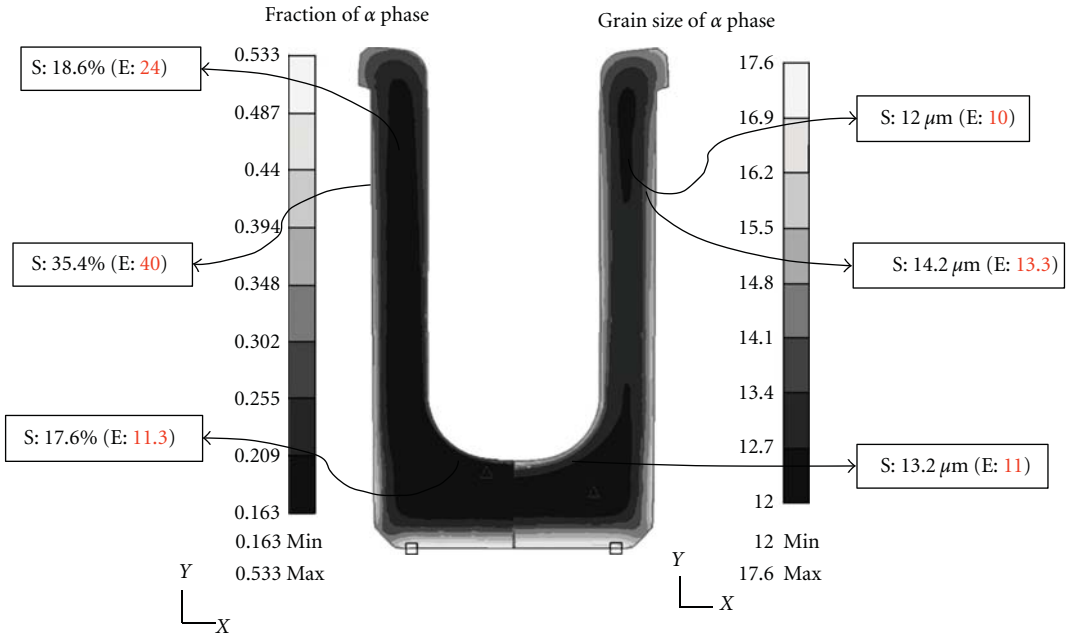

Figure 8: Contours of volume fraction and grain size of primary α phase for hot backward extrusion simulation of Ti-6Al-4V alloy. The symbols "S" and "E" in the bracket denote simulation and experimental results, respectively.

the forming process, and the temperature level at die contact area (or surface area) is lower than that at middle area due to heat transfer between dies and workpiece. Also, the lowest temperature region in the workpiece is found at the bottom, which is in constant contact with the lower die throughout the forming process from the moment the preform is transferred to the die.

Figure 7 shows the Ti-6Al-4V alloy tube manufactured by hot backward extrusion process and the microstructures observed at the cross-section of the tube. It can be found

that extruded Ti-6Al-4V alloy tube is formed without the surface defects. Microstructures observed at most locations indicate a bimodal structure composed of equiaxed α and transformed beta phases. In the microstructural observation from surface to middle positions, it can be seen that the volume fraction of α phase at middle position is smaller than that of α phase at surface.

These microstructure changes during the extrusion process were closely related to the plastic strain and temperature varying at different positions. In this work, in order to predict the α grain size and the α/β phases volume fraction change, the decoupled approach between the microstructure model and FE analysis was applied. The model for predicting the volume fraction change and grain size of α phase was implemented into a post-user-defined subroutine of a commercial FE-code, DEFORM-2D.

Figure 8 shows the comparison between experimental data and simulation results. The experimental data measured from extruded tube were overlapped aside from simulation results. the values in the brackets especially indicate the experimental data. It was found that reasonable accuracy was obtained at most of region and the average deviation was below 15%. Only at a certain part of inner wall, 36% of error was noticed which is due to the contact of the inner wall with the punch occurring in the given microstructures. It is clearly demonstrated that simulation results of volume fraction and grain size of α phase at most locations for the extruded Ti-6Al-4V tube were relatively close to measured values. Consequently, it is suggested that the microstructure simulation module is very useful for hot forming process design of Ti-6Al-4V alloy.

4. Conclusions

In this work, the microstructure evolution of Ti-6Al-4V tube during hot extrusion process was predicted by decoupled approach of FE analysis and microstructure prediction model. In order to evaluate the volume fraction and grain size of α phase during the hot backward extrusion process, the microstructure prediction model of Ti-6Al-4V alloy was suggested and implemented into the post-user subroutine of FE code. The comparison of the microstructure simulation module with the actual microstructures of the backward extruded Ti-6Al-4V alloy tube has successfully validated the reliability of the present module in the prediction of the volume fraction and grain size of α phase.

Acknowledgments

This research was partly supported by a grant through the research program funded by the Agency for Defense Development, Korea, and also partly supported by a grant through the research program (UCN248-2865.C) funded by the Ministry of Knowledge Economy, Korea.

References

[1] X. Duan and T. Sheppard, "Simulation and control of microstructure evolution during hot extrusion of hard aluminium alloys," *Materials Science and Engineering A*, vol. 351, no. 1-2, pp. 282–292, 2003.

[2] J. T. Yeom, J. H. Kim, N. K. Park, S. S. Choi, and C. S. Lee, "Ring-rolling design for a large-scale ring product of Ti-6Al-4V alloy," *Journal of Materials Processing Technology*, vol. 187-188, pp. 747–751, 2007.

[3] J. H. Kim, N. S. Reddy, J. T. Yeom, J. K. Hong, C. S. Lee, and N. K. Park, "Microstructure prediction of two-phase titanium alloy during hot forging using artificial neural networks and fe simulation," *Metals and Materials International*, vol. 15, no. 3, pp. 427–437, 2009.

[4] S. L. Semiatin, V. Seetharaman, and I. Weiss, "The thermomechanical processing of alpha/beta titanium alloys," *JOM*, vol. 49, no. 6, pp. 33–68, 1997.

[5] C. M. Sellars and J. A. Whiteman, "Recrystallization and grain growth in hot rolling," *Metal Science*, vol. 13, no. 3-4, pp. 187–194, 1978.

[6] Z. M. Hu, J. W. Brooks, and T. A. Dean, "Experimental and theoretical analysis of deformation and microstructural evolution in the hot-die forging of titanium alloy aerofoil sections," *Journal of Materials Processing Technology*, vol. 88, no. 1, pp. 251–265, 1999.

[7] S. L. Semiatin, J. C. Soper, and I. M. Sukonnik, "Short-time beta grain growth kinetics for a conventional titanium alloy," *Acta Materialia*, vol. 44, no. 5, pp. 1979–1986, 1996.

[8] S. L. Semiatin, F. Montheillet, G. Shen, and J. J. Jonas, "Self-consistent modeling of the flow behavior of wrought alpha/beta titanium alloys under isothermal and nonisothermal hot-working conditions," *Metallurgical and Materials Transactions A*, vol. 33, no. 8, pp. 2719–2727, 2002.

[9] J. D. Miller and S. L. Semiatin, "Effect of the size distribution of alpha particles on microstructure evolution during heat treatment of an alpha/beta titanium alloy," *Metallurgical and Materials Transactions A*, vol. 36, no. 1, pp. 259–262, 2005.

[10] Y. H. Lee, C. S. Lee, T. J. Shin, S. M. Hwang, and S. M. Shim, "High Temperature Forming of Ti-6Al-4V Alloy Considering Microstructural Evolution," *Key Engineering Materials*, vol. 274–276, pp. 117–122, 2004.

[11] I. T. Yeom, N. K. Park, Y. H. Lee et al., "An improved process design for the hot backward extrusion of Ti-6Al-4V tubes using a finite element method and continuum instability criterion," *Proceedings of the Institution of Mechanical Engineers, Part B*, vol. 221, no. 2, pp. 255–265, 2007.

Hindawi Publishing Corporation
Journal of Metallurgy
Volume 2011, Article ID 959643, 8 pages
doi:10.1155/2011/959643

Research Article

Aging Behaviour of Al-Mg-Si Alloys Subjected to Severe Plastic Deformation by ECAP and Cold Asymmetric Rolling

S. Farè, N. Lecis, and M. Vedani

Dipartimento di Meccanica, Politecnico di Milano, via Giuseppe La Masa, 1, 20156 Milan, Italy

Correspondence should be addressed to M. Vedani, maurizio.vedani@polimi.it

Received 22 March 2011; Accepted 12 June 2011

Academic Editor: Enrico Evangelista

A study was carried out on aging behaviour of a 6082 alloy processed by two different severe plastic deformation techniques: ECAP and asymmetric rolling. Both techniques were able to generate an ultrafine-grained structure in samples processed at room temperature. It was stated that severe straining promotes marked changes in the postdeformation aging kinetics. The peaks of β''/β' transition phases were anticipated and of progressively reduced intensity over the coarse grained alloy. A further peak accounting for onset of recrystallization also appeared in the most severely deformed samples. Full consistency in peak shape and position was found when comparing materials processed by ECAP and asymmetric rolling. Isothermal aging treatments performed at 180°C revealed that in the severely deformed samples, aging became so fast that the hardness curves continuously decreased due to overwhelming effects of structure restoration. On the contrary, aging at 130°C offers good opportunities for fully exploiting the precipitate hardening effects in the ultrafine-grained alloy.

1. Introduction

Wrought Al-Mg-Si alloys (6xxx series aluminum alloys) are widely used for structural applications in aerospace and automotive industries owing to their strength, formability, weldability, corrosion resistance, and cost. The age hardening response of 6xxx series alloys can be very significant, leading to remarkable improvement of strength after an appropriate heat treatment. Their precipitation sequence has been reported in numerous research works, and a satisfactory agreement on phase evolution occurring during aging has been achieved [1–7]. A large number of wrought Al-Mg-Si alloys contain an excess of Si, above that required to form the Mg_2Si (β) phase, to improve the age hardening response. For these alloys, the accepted precipitation sequence starting from a supersaturated solid solution is separate clusters of Si and Mg atoms, coclusters containing Mg and Si atoms, spherical GP zones, needle-like metastable β'' phase, rod-like metastable β' phase, Si precipitates, and platelets of equilibrium β phase. Among these, the β'' precipitates are considered to give the main contribution to strength and hence they are mostly responsible for the peak age hardening effect [2, 4, 5, 8].

Several research works showed that the precipitation kinetics and even precipitation sequence are changed when the alloy structure is plastically deformed. Zhen et al. [5, 9] showed that when Al-Mg-Si alloys had been extensively cold rolled, their aging curves featured a decrease of the precipitation temperatures of some phases. It was suggested that the increased density of defects in the crystal structure would enhance appreciably the diffusion distance of Si and hence promote the formation of a more obvious peak for the GP zones, the anticipation of the metastable β''/β' peak temperatures, and the reduction of the amount of Si and Mg_2Si phases that eventually formed.

Similar modifications in the precipitation sequence were also found in alloys deformed in the severe plastic deformation (SPD) regime, to produce ultrafine-grained alloys. Murayama et al. [10] investigated a solution treated Al-Cu binary alloy processed by equal channel angular pressing (ECAP) to refine its structure at room temperature. By careful DSC and TEM analyses, they stated that during post-ECAP aging, the formation of GP zones and of transition θ'' precipitates was suppressed and that the precipitation of θ' and θ (Al_2Cu) phases was enhanced and occurred at lower temperatures in the heavily deformed structure of

Table 1: Chemical composition (mass %) of the 6082 alloy investigated.

Mg	Si	Mn	Fe	Cu	Cr	Ti	Al
1.193	1.019	0.650	0.267	0.005	0.010	0.015	balance

the alloys. Huang and coworkers [11] consistently stated that in a laboratory Al-4 wt.% Cu alloy severely deformed after solution annealing, copious precipitation of θ phase occurred at grain boundaries on natural aging, while no indication of θ'', θ', or GP zones formation was observed. Gubicza et al. [12] obtained similar conclusions on supersaturated Al-Zn-Mg alloys processed by ECAP at 200°C. They observed that high-temperature straining suppresses the formation of GP zones and η' transition precipitates while enhancing the precipitation kinetics of the η precipitates over the conventionally solution treated and artificially aged alloys.

Information on aging response of SPD-processed 6xxx alloys is also available. Roven and coauthors [8] investigated the precipitation behaviour of a 6063 alloy during ECAP at RT and at 175°C and found that spherical β'' precipitates are dynamically formed from the as-solutionized alloy during SPD even at RT, instead of the needle-like β'' transition precipitates that are usually observed in conventionally aged alloys. Some of the present authors [13, 14] investigated the aging behaviour of several wrought alloys of the Al–Mg–Si system after ECAP and showed that precipitation kinetics in the ultrafine-grained alloys was markedly accelerated over the coarse-grained materials. It was also demonstrated that the formation of β''/β' phases occurred at lower temperatures with increasing ECAP strain, whereas β' precipitation was strongly reduced due to expected formation of competing Si-rich phases in the heavily deformed structure.

In the present paper, comparative results are presented on post-SPD aging behaviour of a commercial 6082 Al alloy severely deformed at room temperature by two different techniques. Available data on ECAP processed alloys in the as-solution annealed condition are compared to results obtained on the same materials deformed by asymmetric rolling. Investigations on aging kinetics and structure development allowed to draw conclusions on aging behaviour aimed at defining optimal parameters and treatment feasibility for ultrafine-grained Al-Mg-Si alloys.

2. Materials and Experimental Procedures

A commercial 6082 Al alloy supplied in the form of extruded bars was investigated. The alloy chemical composition is given in Table 1.

For ECAP processing, samples having a length of 100 mm and a diameter of 10 mm were cut from the bars, solution treated in a muffle furnace at 530°C for 2 hours and water quenched.

ECAP pressing was carried out using a die with channels intersecting at an angle Φ of 90° and with an external curvature angle Ψ of 20°, corresponding to a theoretical strain of 1.05 for each pass [15]. Samples were processed at room temperature by the so-called route C (rotation by 180° of the specimen at each pass) to accumulate up to six passes. The experimental details of the ECAP facility and material processing are described elsewhere [16].

For asymmetric rolling (ASR) in the SPD regime, samples having a thickness of 20 mm and width of 40 mm were cut and subjected to the same solution treatment above mentioned. Cold rolling reduction was performed down to a thickness of 0,23 mm by a multipass procedure with no intermediate annealing treatments. The rolling schedule consisted of thickness reductions of about 20% at each step and the rotation of the billet along its longitudinal axis before each pass (a procedure equivalent to route C adopted for ECAP). The asymmetry ratio, namely, the rotational speed ratio between the two rolls, was set to 1,4 on the basis of previous studies [17]. A laboratory rolling mill in a two-high configuration, featuring the possibility of independently modifying the rotational speed of the rolls, was adopted for this purpose.

Analyses on grain structure evolution and on precipitates developed in SPD processed and aged samples was performed by TEM. Disk samples were prepared by cutting disks from ECAP billets and rolled samples, manually grinding and polishing. Twin jet electrolytic thinning was then carried out at −35°C with a 30% HNO_3 solution in methanol at 18 V.

Samples of the processed alloy were subjected to DSC analyses to investigate the influence of SPD on precipitation kinetics. Runs were carried out on samples having a weight of about 50 mg in a purified argon atmosphere with a scanning rate of 20°C/min. The effects associated to transformation reactions were isolated by subtracting a baseline recorded form high-purity Al runs.

Vickers microhardness adopting a load on the indenter of 1 N was adopted to evaluate modification of alloy strength. Evolution of microhardness was assessed as a function of aging time during isothermal treatments at temperatures of 180 and 130°C. The profiles allowed to state the peak-hardness aging times of the processed alloy as a function of the strain imparted either by ECAP or by ASR. Comparative results are presented in this paper considering the equivalent strain experienced. For ECAP, the Iwahashi equivalent strain was calculated [15] whereas for ASR, the equivalent Von Mises strain was evaluated, assuming plane strain deformation [18], by

$$\varepsilon_{\text{eq}} = \frac{2}{\sqrt{3}} \cdot \ln\left(\frac{h_0}{h_f}\right) \cdot \varnothing, \tag{1}$$

with h_0 and h_f being the initial and final thickness, respectively, and $\varnothing$ a parameter accounting for the asymmetry effects.

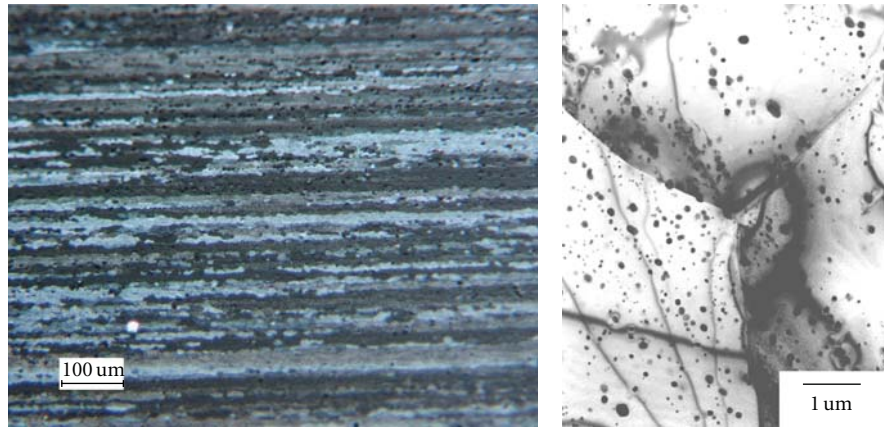

(a) (b)

Figure 1: Microstructure of the coarse grained 6082 Al alloy before SPD. (a) Optical and (b) TEM micrographs.

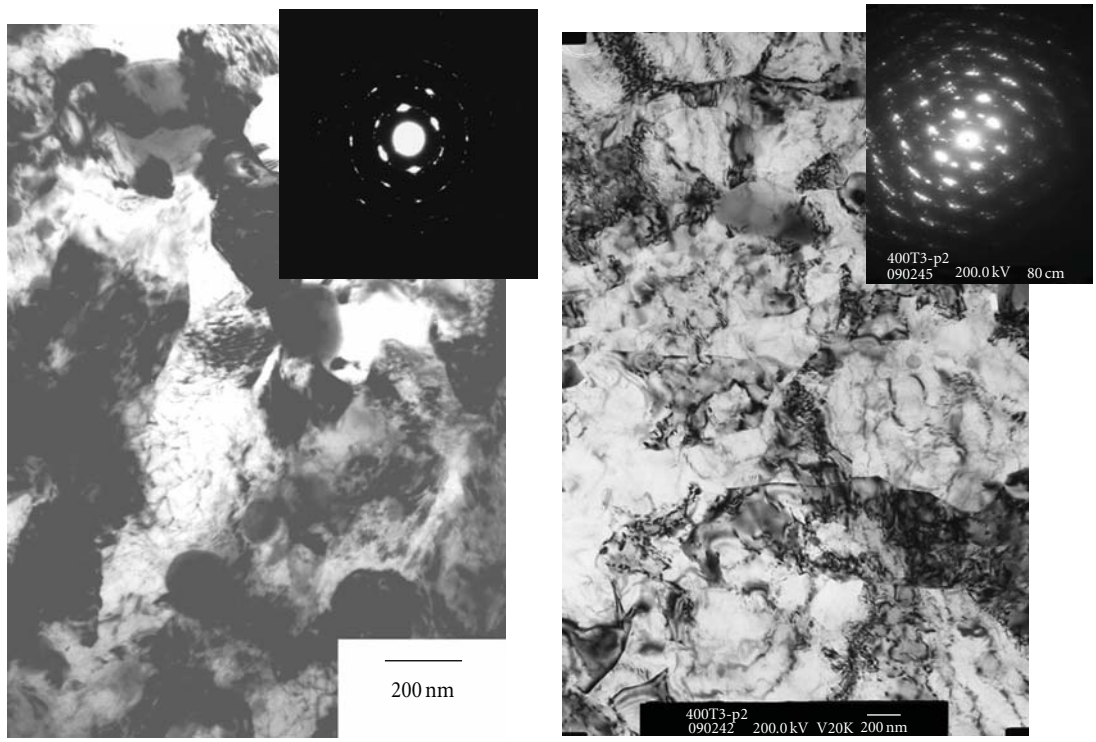

(a) (b)

Figure 2: Representative TEM images and corresponding SAD patterns of the ultrafine structure achieved after (a) 6 ECAP passes and (b) asymmetric rolling reduction corresponding to 5,50 equivalent strain.

3. Results and Discussion

3.1. Grain Structure after SPD. In Figures 1 and 2, sets of representative micrographs showing the initial solution annealed coarse structure and its evolution toward the ultrafine scale by ECAP and ASR are reported. Details of the microstructure evolution during ECAP and ASR processing have already been published elsewhere [13, 17]. It is worth considering here that for both processes, after the first passes, sets of parallel bands of subgrains a few hundreds of micrometers in width are formed. By increasing the number of passes, the subboundary misalignment increased (as inferred by the increased spreading of the spots of the SAD patterns). Eventually, subgrain fragmentation and further increase of the misalignment led to an ultrafine equiaxed high-angle grain structure. For both processes, the average grain size achieved after the highest imparted strain (6 ECAP passes corresponding to an equivalent strain of 6,33 and

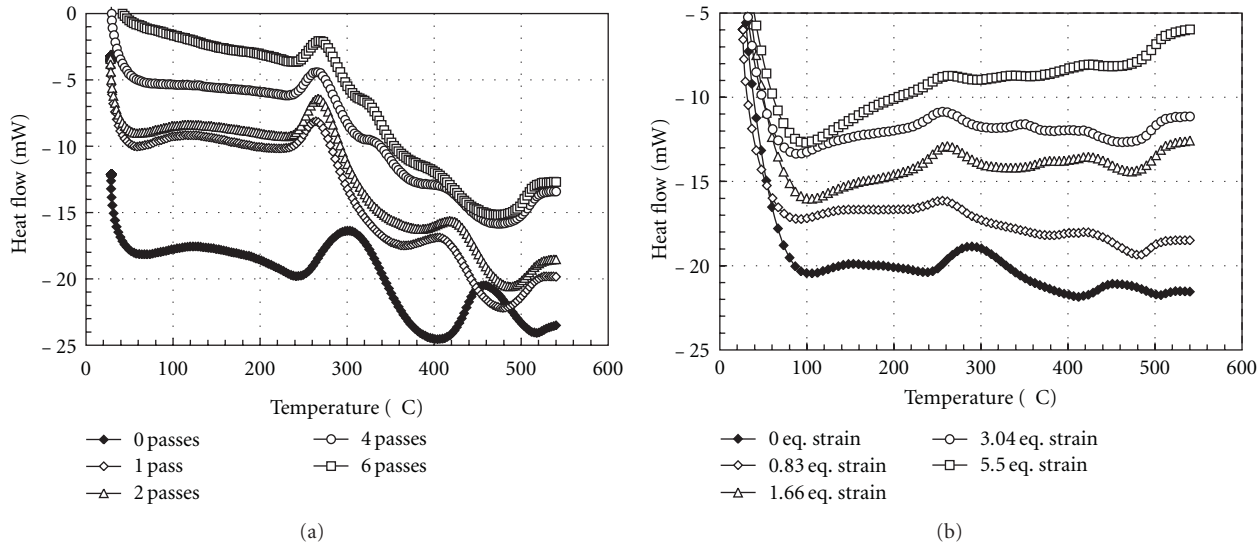

Figure 3: DSC curves of the solution annealed and SPD processed 6082 alloy as a function of (a) ECAP passes and (b) amount of equivalent strain imparted by ASR. The curves are arbitrarily shifted along y-axis to avoid superposition.

reduction down to a thickness of 0,23 mm, corresponding to an equivalent strain of 5,50 for asymmetric rolling) was of about 300 nm.

3.2. Differential Scanning Calorimetry. Figure 3 summarizes typical DSC runs recorded as a function of ECAP passes and equivalent strain given by ASR of the solution-treated 6082 alloy. The thermograms of the unprocessed solution treated alloy match the established aging sequence of this alloy [1–3, 9]. In particular, the broad exothermic peak (upward peak) in the plot of Figure 3(a) at 305°C, often interpreted as two partially superimposed subpeaks, corresponds to the formation of β'' and β' metastable precipitates at about 270°C and 330°C, respectively. More specifically, it was suggested that the subpeak at 270°C could also be related to precipitation of tiny Si-rich particles acting as precursors for the formation of the β'' phase and that the peak at 330°C corresponds to formation of both rod-shaped β' phase and relatively large Si-rich precipitates [1, 2, 9]. A dissolution endothermic trough (downward peak in the plot) of the above phases follows at about 400°C, while the second marked exothermic peak at 460°C and the corresponding endothermic trough at 520°C are related to the formation and dissolution of the equilibrium β-Mg_2Si phase.

The ECAP processed alloys (see Figure 3(a)) feature marked differences in position and shape of the peaks. The above described broad peak related to the formation of β'' and β' phases now appears as a more narrow peak centred at 275°C, irrespective of the number of ECAP passes experienced. The formation of the stable β precipitates in the severely deformed alloy revealed to be markedly anticipated (405–415°C) and of progressively reduced intensity with respect to the unprocessed solution treated alloy. It is also worth noting that a new peak appears at about 330°C in the alloy processed to 4 and 6 ECAP passes and in ASR samples deformed to similar equivalent strains (see arrows in Figures 3(a) and 3(b)). In a previous study, some of the present authors focussed on the interpretation of aging peaks of ECAP processed Al-Mg-Si alloys of similar composition [14]. By TEM analysis of samples aged in the DSC just immediately before the onset, and after the offset of this peak, they were able to demonstrate that this unexpected hump detected in the most strain-hardened samples was related to recrystallization phenomena that became more evident and developed at decreasing temperatures as ECAP strain increased.

Finally, comparison between Figures 3(a) and 3(b) supplies evidence about similarities of effects promoted by ECAP and ASR processes. Inspection of the thermograms reveals full consistency of peak positions as a function of strain (it is to remind that each ECAP pass corresponds to a strain of 1,05) for the two SPD techniques here considered. The only difference concerns the amplitude of precipitate peaks that is supposed to be due to different weight of samples. Indeed, due to geometrical constraints, the samples cut from the ASR thin sheets had a less regular shape with a higher surface/volume ratio.

While information on ECAP effects on aging was already available in the literature owing to a number of published research studies [8, 10–12, 19], data on aging behaviour in Al alloys severely deformed by cold rolling are relatively less frequent. The present data on aging of ASR performed in the severe deformation regime (up to 5,50 equivalent strain) are indeed in good agreement with established evidence showing that kinetics and morphology of transition precipitates are deeply altered by SPD and that new opportunities for isothermal aging at lower temperatures deserve to be explored owing to accelerated diffusion of alloying elements in the heavily dislocated alloy structure. It is worth mentioning that studies were carried recently on 6061 and 6063 Al alloys subjected to room temperature and cryogenic rolling in the severe plastic deformation regime [20, 21].

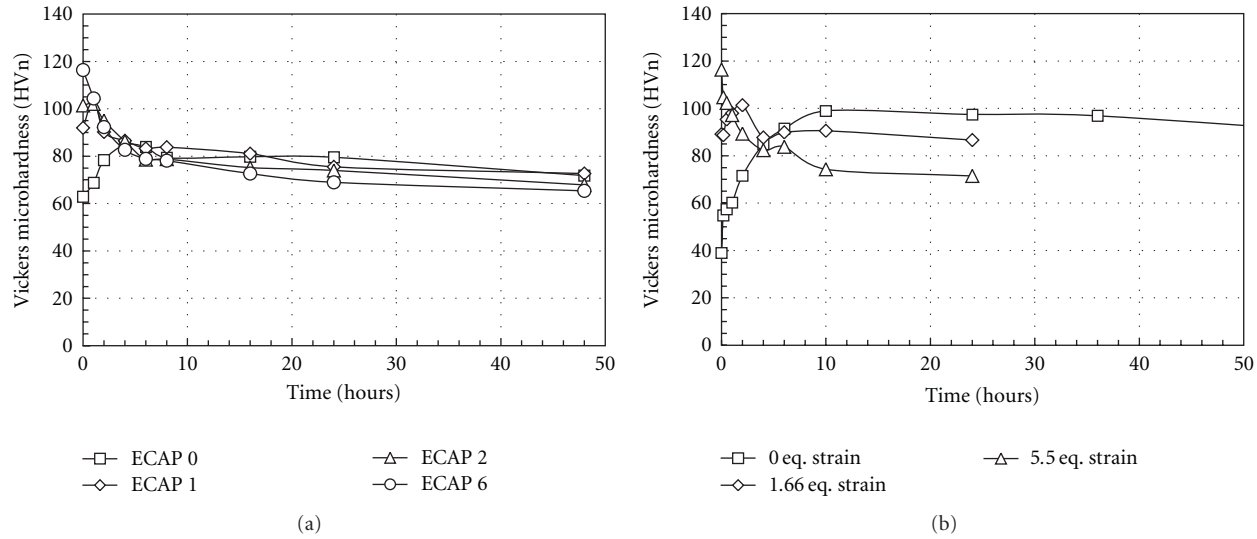

Figure 4: Aging curves at 180°C of the solution annealed and SPD processed 6082 alloy as a function of (a) ECAP passes and (b) amount of equivalent strain imparted by ASR.

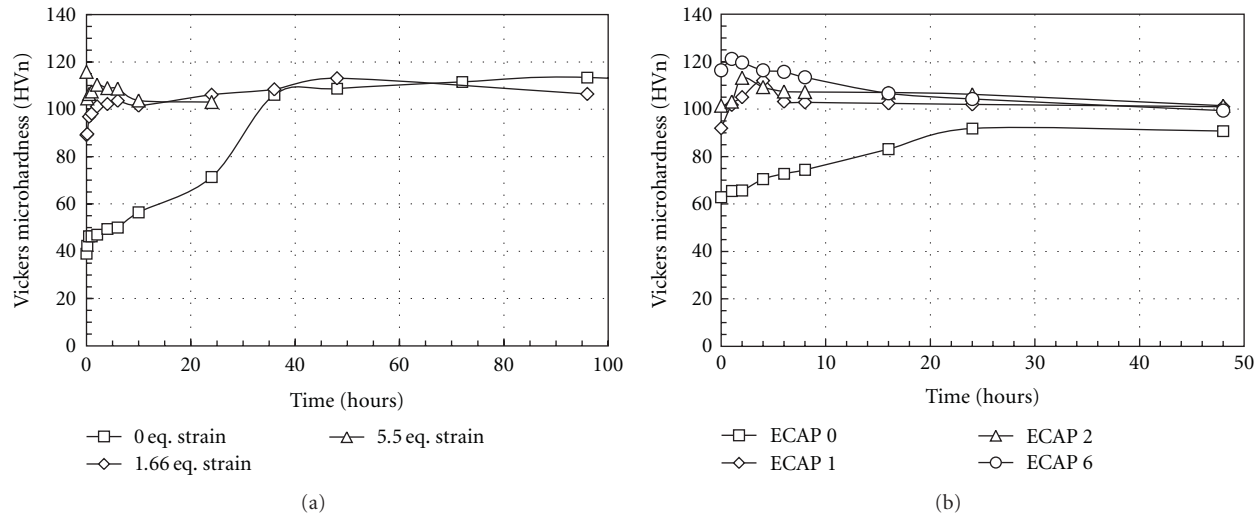

Figure 5: Aging curves at 130°C of the solution annealed and SPD processed 6082 alloy as a function of (a) ECAP passes and (b) amount of equivalent strain imparted by ASR.

It was observed that low-temperature processing causes substantial suppression of structure recovery during straining and hence preserves higher dislocation densities in the samples, increasing the driving force for sub-microcrystalline grain development. This feature was more significant when presolution annealed alloys were processed due to effects of solute elements (mainly Mg and Si for 6xxx series alloys) in pinning dislocations and retarding their annihilation during deformation.

A further issue related to aging of UFG structures was considered by Chinh and coauthors [22] who proposed several strategies for processing age-hardenable alloys. It was stated that for Al-Mg-Zn-Zr alloys, ECAP processing should be performed immediately after quenching or at least within a very short period of preaging, to avoid excessive strengthening effects related to anticipated aging and hence formation of cracks during further ECAP passes.

3.3. Aging Kinetics. Post-SPD aging behaviour was further investigated by isothermal treatments at 130 and 180°C. The evolution of microhardness as a function of aging time at the above-mentioned temperatures is depicted in Figures 4 and 5.

When comparing the peak-hardness times as a function of the amount of strain experienced by the alloy prior to the aging treatment, it is readily confirmed that severe plastic deformation remarkably accelerates the aging kinetics, consistently with previous DSC results. For the alloy processed to the highest strain levels (e.g., 6 passes by ECAP and 5,50 equivalent strain by ASR), aging at 180°C became so fast

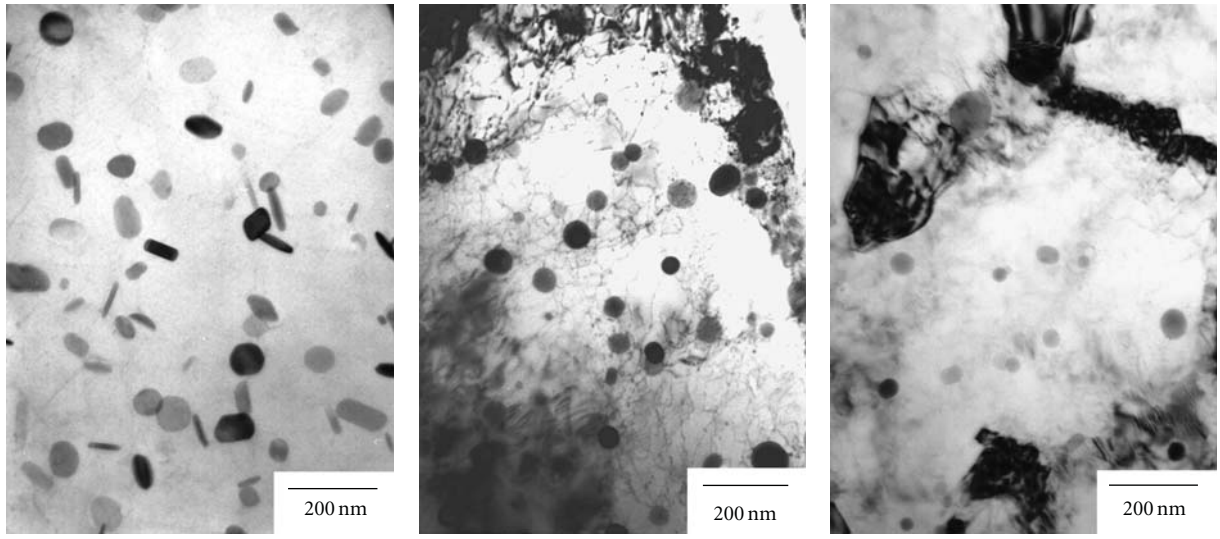

Figure 6: Morphology of strengthening precipitates detected in (a) solution annealed and peak aged coarse-grained alloy, (b) presolution annealed and peak-aged after 1 ECAP pass, (c) presolution annealed and peak-aged after 6 ECAP passes [13].

that the hardness curves continuously decreased, starting from beginning of the aging treatment (see Figure 4). It must be considered that during aging, recovery of the heavily deformed structure and precipitation from the supersaturated solution can simultaneously occur. The former mechanism lowers defect density, which results in decreasing strength, the latter contributes to increased density of dispersoids and hence improves the strengthening effect. The continuous loss of hardness detected during aging at 180°C here reported is therefore supposed to be due to overwhelming restoration mechanisms of the deformed structure over the precipitation hardening potential, in good accordance with other literature reports [19]. The data shown in Figure 5 suggests that isothermal aging carried out at 130°C on presolutionised and SPD processed alloys could supply interesting opportunities for fully exploiting the precipitate hardening effects while controlling the stored energy in the structure. This evidence is confirmed by investigations carried out by Panigrahi et al. [21] and by Niranjani et al. [23] showing that even temperatures as low as 100°C can be successfully selected for aging of Al–Mg–Si alloys after severe plastic deformation by rolling. Nikitina et al. [24] considered an Al-Cu-Mg-Si alloy processed by HPT and investigated structural stability and aging behaviour of the UFG alloy. Also these authors found evidence of a markedly anticipated aging behaviour by DSC and highlighted by microhardness measurements that the SPD processed samples underwent significant softening during treatments at temperatures exceeding 175°C even for aging times as low as 30 minutes.

From present data, it can be suggested that a proper combination of grain-refinement strengthening and age-hardening can be fully exploited in solution annealed UFG alloys only when isothermal aging is performed at temperatures significantly lower than conventional values and for shorter periods that have to be tailored to specific amount of strain imparted during SPD and alloy composition. Stability of UFG structure would also be preserved by the addition of dispersoid-forming elements that could retard restoration during aging [14].

3.4. Strengthening Precipitates. Investigation on the strengthening precipitate structure found in the SPD processed samples was carried out only on a limited number of ECAP conditions [13]. Figure 6 depicts a colletion of TEM micrographs taken from ECAP samples peak aged at 130°C. The peak aging time of each condition was selected on the basis of the hardness curves previously reported in Figure 5(a). The solution annealed and peak aged 6082 alloy (undeformed sample) featured a dispersion of about 0,1 μm long rod-like phases identified as β' precipitates on the basis of their morphology [1, 2] together with globular particles with an average size of 50 nm. In the ECAP processed samples shown in Figures 6(b) and 6(c), arrangement of dislocation in the matrix was observed according to expected recovery mechanisms acting during aging. Moreover, the above-mentioned globular particles became predominant over the rod-like precipitates.

4. Conclusions

A study was carried out on aging of a 6082 alloy processed by two different severe plastic deformation techniques. From comparative analysis of the results, the following conclusions can be drawn.

(i) Both ECAP and ASR were able to generate an ultrafine structure consisting of equiaxed grains after extensive deformation at room temperature. At the highest strain investigated, of 6 ECAP passes (corresponding to an equivalent strain of 6,33) and of an equivalent strain of 5,50 given by ASR, an average grain size of about 300 nm was detected.

(ii) DSC analyses revealed that SPD carried out on the presolution annealed alloy promotes marked changes in the postdeformation aging kinetics. The peaks of β''/β' transition phases were anticipated and of progressively reduced intensity over the conventional coarse grained (not processed by SPD) alloy. A peak accounting for onset of recrystallization also appeared in samples deformed for more than 4 passes by ECAP or rolled by ASR at equivalent strains exceeding 3. A full consistency in peak shape and position was found when comparing materials processed by the two SPD techniques and strained at comparable levels.

(iii) Isothermal aging treatments performed at 130 and 180°C on the presolution annealed and SPD processed samples were considered to establish optimal aging times and to evaluate the achievable strength by microhardness. It was confirmed that SPD remarkably accelerates the aging kinetics. For the alloy processed to the highest strain levels, aging at 180°C became so fast that the hardness curves continuously decreased due to overwhelming effects of structure restoration. On the contrary, aging carried out at 130°C offered good opportunities for fully exploiting the precipitate hardening effects, while preserving the ultrafine-grained structure.

(iv) TEM investigations performed on selected samples aged at 130°C to peak hardness condition showed that the rod-like β' transition phase typically found in the coarse grained samples was progressively replaced by globular precipitates in ultrafine SPD processed samples.

(v) The experimental data here presented suggest that a proper combination of grain-refinement strengthening and age-hardening can be fully exploited in solution annealed UFG alloys only when isothermal aging is performed at temperatures significantly lower than conventional values and for shorter periods. Aging conditions have to be tailored to specific amount of strain imparted during SPD and to alloy composition.

Acknowledgments

The authors would like to thank Dr. G. Angella for TEM analyses. This research was partially financed by MIUR within the framework of PRIN projects under Grant 2008YNZB7M.

References

[1] K. Gupta, D. J. Lloyd, and S. A. Court, "Precipitation hardening in Al-Mg-Si alloys with and without excess Si," *Materials Science and Engineering A*, vol. 316, no. 1-2, pp. 11–17, 2001.

[2] G. A. Edwards, K. Stiller, G. L. Dunlop, and M. J. Couper, "The precipitation sequence in Al-Mg-Si alloys," *Acta Materialia*, vol. 46, no. 11, pp. 3893–3904, 1998.

[3] K. Matsuda, Y. Sakaguchi, Y. Miyata et al., "Precipitation sequence of various kinds of metastable phases in Al-1.0mass% Mg2Si-0.4mass% Si alloy," *Journal of Materials Science*, vol. 35, no. 1, pp. 179–189, 2000.

[4] M. Takeda, F. Ohkubo, T. Shirai, and K. Fukui, "Stability of metastable phases and microstructures in the ageing process of Al-Mg-Si ternary alloys," *Journal of Materials Science*, vol. 33, no. 9, pp. 2385–2390, 1998.

[5] L. Zhen, W. D. Fei, S. B. Kang, and H. W. Kim, "Precipitation behaviour of Al-Mg-Si alloys with high silicon content," *Journal of Materials Science*, vol. 32, no. 7, pp. 1895–1902, 1997.

[6] M. Murayama and K. Hono, "Pre-precipitate clusters and precipitation processes in Al-Mg-Si alloys," *Acta Materialia*, vol. 47, no. 5, pp. 1537–1548, 1999.

[7] G. Biroli, G. Caglioti, L. Martini, and G. Riontino, "Precipitation kinetics of AA4032 and AA6082: a comparison based on DSC and TEM," *Scripta Materialia*, vol. 39, no. 2, pp. 197–203, 1998.

[8] H. J. Roven, M. Liu, and J. C. Werenskiold, "Dynamic precipitation during severe plastic deformation of an Al-Mg-Si aluminium alloy," *Materials Science and Engineering A*, vol. 483-484, no. 1-2 C, pp. 54–58, 2008.

[9] S. B. Kang, L. Zhen, H. W. Kim, and S. T. Lee, "Effect of cold rolling and aging treatment on mechanical property and precipitation behavior in a Al-Mg-Si alloy," *Materials Science Forum*, vol. 217-222, no. 2, pp. 827–832, 1996.

[10] M. Murayama, Z. Horita, and K. Hono, "Microstructure of two-phase Al-1.7 at% Cu alloy deformed by equal-channel angular pressing," *Acta Materialia*, vol. 49, no. 1, pp. 21–29, 2001.

[11] Y. Huang, J. D. Robson, and P. B. Prangnell, "The formation of nanograin structures and accelerated room-temperature theta precipitation in a severely deformed Al-4 wt.% Cu alloy," *Acta Materialia*, vol. 58, no. 5, pp. 1643–1657, 2010.

[12] J. Gubicza, I. Schiller, N. Q. Chinh, J. Illy, Z. Horita, and T. G. Langdon, "The effect of severe plastic deformation on precipitation in supersaturated Al-Zn-Mg alloys," *Materials Science and Engineering A*, vol. 460-461, pp. 77–85, 2007.

[13] G. Angella, P. Bassani, A. Tuissi, and M. Vedani, "Aging behaviour and mechanical properties of a solution treated and ECAP processed 6082 alloy," *Materials Transactions*, vol. 45, no. 7, pp. 2282–2287, 2004.

[14] M. Vedani, G. Angella, P. Bassani, D. Ripamonti, and A. Tuissi, "DSC analysis of strengthening precipitates in ultrafine Al-Mg-Si alloys," *Journal of Thermal Analysis and Calorimetry*, vol. 87, no. 1, pp. 277–284, 2007.

[15] Y. Iwahashi, J. Wang, Z. Horita, M. Nemoto, and T. G. Langdon, "Principle of equal-channel angular pressing for the processing of ultra-fine grained materials," *Scripta Materialia*, vol. 35, no. 2, pp. 143–146, 1996.

[16] M. Vedani, P. Bassani, M. Cabibbo, and E. Evangelista, "Experimental aspects related to equal channel angular pressing of a commercial AA6082 alloy," *Metallurgical Science and Technology*, vol. 21, p. 3, 2003.

[17] S. Farè, M. Vedani, and G. Angella, "Features on grain-structure evolution during asymmetric rolling of aluminium alloys," *Materials Science Forum*, vol. 604-605, pp. 77–85, 2009.

[18] Q. Cui and K. Ohori, "Grain refinement of high purity aluminium by asymmetric rolling," *Materials Science and Technology*, vol. 16, no. 10, pp. 1095–1101, 2000.

[19] E. Cerri and P. Leo, "Influence of severe plastic deformation on aging of Al-Mg-Si alloys," *Materials Science and Engineering A*, vol. 410-411, pp. 226–229, 2005.

[20] W. J. Kim, J. Y. Wang, S. O. Choi, H. J. Choi, and H. T. Sohn, "Synthesis of ultra high strength Al-Mg-Si alloy sheets by differential speed rolling," *Materials Science and Engineering A*, vol. 520, no. 1-2, pp. 23–28, 2009.

[21] S. K. Panigrahi, R. Jayaganthan, and V. Pancholi, "Effect of plastic deformation conditions on microstructural characteristics and mechanical properties of Al 6063 alloy," *Materials and Design*, vol. 30, no. 6, pp. 1894–1901, 2009.

[22] N. Q. Chinh, J. Gubicza, T. Czeppe et al., "Developing a strategy for the processing of age-hardenable alloys by ECAP at room temperature," *Materials Science and Engineering A*, vol. 516, no. 1-2, pp. 248–252, 2009.

[23] V. L. Niranjani, K. C. Hari Kumar, and S. Subramanja Sarma, "Development of high strength Al-Mg-Si AA6061 alloy through cold rolling and ageing," *Materials Science and Engineering A*, vol. 515, no. 1-2, pp. 169–174, 2009.

[24] M. A. Nikitina, R. K. Islamgaliev, and A. F. Kamalov, "Thermal stability of the ultrafine-grained Al-Cu-Mg-Si aluminum alloy," *Reviews on Advanced Materials Science*, vol. 25, no. 1, pp. 74–81, 2010.

Hindawi Publishing Corporation
Journal of Metallurgy
Volume 2011, Article ID 165307, 10 pages
doi:10.1155/2011/165307

Research Article

Transition in Deformation Mechanism of AZ31 Magnesium Alloy during High-Temperature Tensile Deformation

Masafumi Noda,[1] Hisashi Mori,[2] and Kunio Funami[1]

[1] *Department of Mechanical Science and Engineering, Chiba Institute of Technology, 2-17-1, Tsudanuma, Narashino, Chiba 275-0016, Japan*
[2] *Materials Technology Division, Railway Technical Research Institute, 2-8-38, Hikari-machi, Kokubunji, Tokyo 185-8540, Japan*

Correspondence should be addressed to Hisashi Mori, forest@rtri.or.jp

Received 24 December 2010; Revised 20 April 2011; Accepted 6 May 2011

Academic Editor: Chong Soo Lee

Magnesium alloys can be used for reducing the weight of various structural products, because of their high specific strength. They have attracted considerable attention as materials with a reduced environmental load, since they help to save both resources and energy. In order to use Mg alloys for manufacturing vehicles, it is important to investigate the deformation mechanism and transition point for optimizing the material and vehicle design. In this study, we investigated the transition of the deformation mechanism during the high-temperature uniaxial tensile deformation of the AZ31 Mg alloy. At a test temperature of 523 K and an initial strain rate of $3 \times 10^{-3}\,s^{-1}$, the AZ31 Mg alloy (mean grain size: $\sim 5\,\mu m$) exhibited stable deformation behavior and the deformation mechanism changed to one dominated by grain boundary sliding.

1. Introduction

Recently, there has been a strong demand for measures that can be adopted to improve the energy efficiency of vehicles and to reduce CO_2 emission. One such measure involves further reducing the weight of members or devices in vehicles [1–3]. Possible measures for weight reduction include reducing the number of vehicle parts, decreasing the member thickness, and using light materials. Another approach is to use Mg alloys, which are the lightest and the most promising metallic materials [4–6]. Thus, Mg alloys have been widely used in thixomolding and casting products [7, 8]. To increase the utility of these alloys, attempts to increase their strength and formability have been made [9–12]. Mg alloys have been used in vehicles, and they have recently been used as secondary strength members in cell phones, electronic devices, and so forth [13, 14]. Increasing the use of Mg alloys in the vehicle members of transport devices involves many challenges, including optimizing the plastic working and strengthening the alloys to allow the fabrication of members with various shapes.

Cold working is known to be a difficult process for conducting the plastic working of Mg alloys since the deformability of the alloys is extremely small at room temperature, because of the hexagonal close-packed structure of Mg alloys [15]. However, Mg alloys with a slip system other than the basal slip system can become more active; this results in a lower deformation resistance and a considerable increase in expansion when the deformation temperature increases. Therefore, considering the product precision and formability, plastic working of Mg alloy members is conducted mostly at high temperatures [16]. There are many reports on the strength, elongation, and superplasticity of Mg alloys [17–19]. However, to develop plastic working technology for Mg alloys, it is important to study the high-temperature deformation behavior of Mg alloys and their drawability and extrusion properties. The majority of studies on Mg alloys such as the Mg-Zn-Y [20, 21] and Mg-Zn-Gd [22, 23] alloys have neither addressed the development of technology for controlling the working nor included a detailed analysis of the deformation behavior. Furthermore, few researchers have reported on the transition points

where the high-temperature deformation behavior of the AZ31 Mg alloy changes, although superplastic deformation has been investigated [24–27]. Therefore, in this study, we examined the transition points of the deformation mechanism observed under high-temperature deformation by conducting high-temperature uniaxial tensile tests on rolled AZ31 material and by evaluating the stability of the deformation mechanism during high-temperature deformation. The objective is to develop a plastic working technology for the AZ31 Mg alloy.

2. Experimental Procedure

The tensile specimen was an extruded rod of the AZ31 Mg alloy (rod diameter: 70 mm; rod length: 800 mm). The chemical composition of the rod (in mass%) was as follows: Al, 3.0%; Zn, 0.89%; Mn, 0.5%; Cu, 0.0016%; Si, 0.028%; Fe, 0.002%; and Mg constituted the rest of the mass. Figure 1 shows an optical micrograph of the extruded material. The grain size of the extruded material was 27 μm. We cut out the rolled material from the extruded rod material such that it had a thickness of 5 mm, a length of 50 mm, and a width of 50 mm; the cutting was performed by machining. The rolled material was then homogenized by maintaining it at 573 K for 1.8 ks in an electric furnace and cooling it in water. After homogenization, the rolled material was maintained for 0.36 ks in an electric furnace heated to 493 K and subjected to multipass rolling (rolling temperature: 493 K; rolling rim speed: 0.17 m/s). Rolling was conducted so that the thickness would be progressively reduced from 5.0 to 2.5, 1.5, and 1.0 mm, and the material was reheated in an electric furnace for 0.18 ks when each pass was completed. The material was cooled in water after the thickness decreased to 1.0 mm. Longitudinal section observations showed that the rolled plate had an isometric grain diameter of approximately 5 μm. A tensile specimen with a gauge length, width, and thickness of 8, 4, and 1 mm, respectively, was obtained from the rolled material. Here, the direction of material extrusion, direction of rolling, and tensile direction were parallel. For the high-temperature tensile test conducted in an Ar atmosphere, the range of test temperatures was set to 523 to 623 K, the range of initial strain rates was set to 3×10^{-1} to 3×10^{-4} s^{-1}, and the rate of temperature increase was set to 0.17 K s^{-1}. The temperature was maintained for 0.9 ks when the target temperature was reached. After deformation, the structure was observed by optical microscopy and by field-emission scanning electron microscopy (FE-SEM). Figure 2 shows an optical micrograph of the longitudinal section structure, the inverse pole figure (IPF) map, and the pole figure (PF) map of the hot-rolled plate obtained by electron backscatter diffraction (EBSD). The EBSD analysis was conducted using a measured view of 150 μm $\times$ 150 μm in 0.3 μm steps. Figure 2(c) shows that the rolled material had a basal texture with a maximum intensity of 6.3 at 80% rolling reduction. The basal texture is considered to have developed because the number of passes was three and rolling was conducted at 493 K with reheating within a short period. The intensity of the basal texture and that of the sheet rolled using a single roller when the AZ31 Mg alloy was subjected to working from 473 to 673 K until the rolling reduction reached 85.7% were found to be 7 and 5, respectively, although the grain is isometric [28].

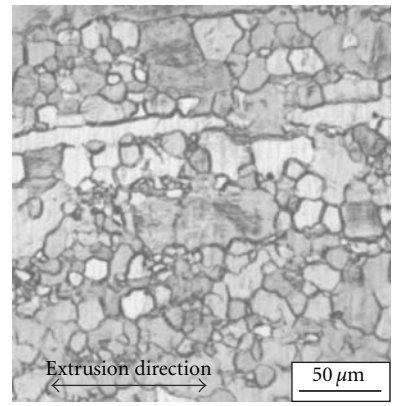

Figure 1: Optical micrograph of the as-extruded material.

3. Results

3.1. Mechanical Properties of High-Temperature Tensile Deformation. To study the effects of test temperatures and strain rate on tensile deformation, the nominal-stress-nominal-strain curve at test temperatures of 523, 573, and 623 K for initial strain rates of 3×10^{-1} s^{-1} to 3×10^{-4} s^{-1} are shown in Figure 3. The stress-strain behavior shows an increase in stress with concurrent work hardening during the initial stages of tensile deformation; the stress then reached a maximum, after which the tensile specimen broke and the stress decreased because of work hardening [29].

At the high strain rates in the range we considered, the tensile specimen broke suddenly after it showed the maximum stress. However, the level of work hardening as well as the maximum stress decreased as the initial strain rate decreased and the test temperature increased; a stationary deformation area and massive extension were observed under low stress. These behaviors are consistent with the high-temperature deformation and superplastic behavior of AZ-type Mg alloys [30, 31], Mg-RE (rare-earth) alloys [32, 33], and Al-Mg alloys [34].

3.2. Effects of Strain Rate and Temperature on Breaking Elongation and Maximum Stress. Figure 4 shows the effects of test temperature and strain rate on breaking elongation. The breaking elongation tended to increase as the initial strain rate decreased and the test temperature increased. At the high initial strain rate of 3×10^{-1} s^{-1}, the breaking elongation was nearly 100%, regardless of the test temperature.

Figure 5 shows the effect of the test temperature and strain rate on deformation stress. Since the rigidity modulus is affected by the temperature, the deformation stress shown is normalized with the rigidity modulus at the maximum stress [35, 36]. The rigidity modulus was calculated on the

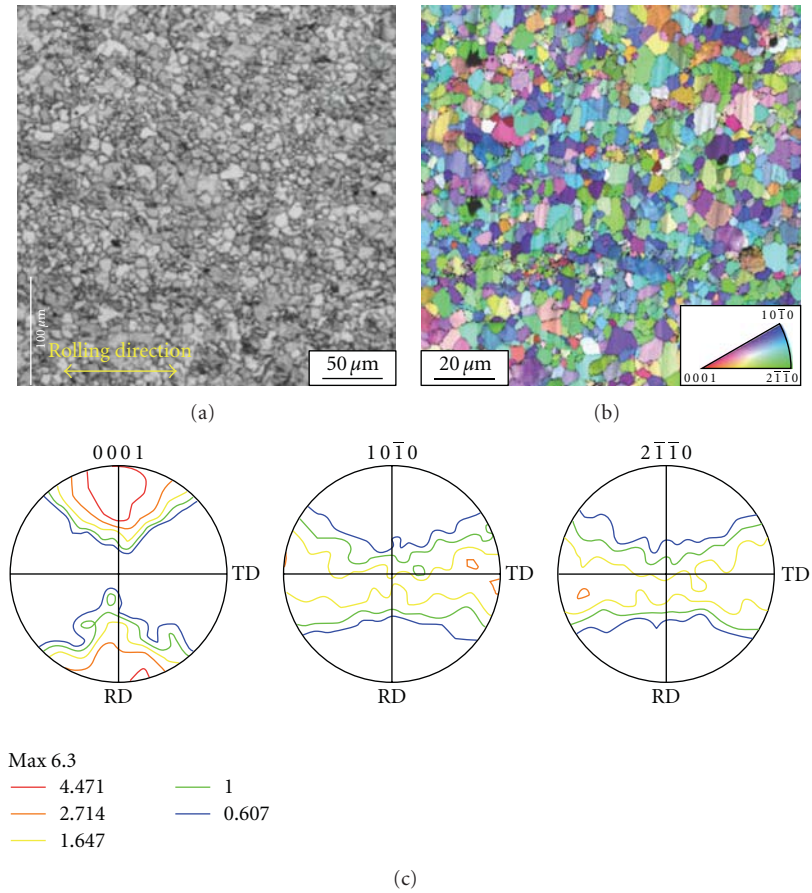

Figure 2: Optical micrograph (a), inverse pole figure map (b), and pole figure map (c) of the as-rolled specimens.

basis of the relationship between the rigidity modulus and temperature given by the following equation:

$$\mu = \mu_0\left(1 + \left(\frac{T - 300}{T_M}\right)\left(\frac{T_M d\mu}{\mu_0 dT}\right)\right). \quad (1)$$

Here, μ denotes the rigidity modulus at a certain temperature (T), μ_0: the initial rigidity modulus (1.6×10^4 (MNm^{-2}) for Mg), T_M, the melting point (924 K), and ($T_M\delta\mu/\mu_0\delta T$), a constant equal to -0.49. The double-logarithmic relationship between the initial strain rate and maximum stress normalized by the rigidity modulus was linear, as shown in Figure 5. It is evident that the normalized maximum stress decreases as the test temperature increases and the strain rate decreases. We calculated the stress exponent (n) from the gradient of this linear relationship and found that the value of n is 2 at 573 K and 623 K and strain rates of 3×10^{-3} to 10^{-4} s^{-1}; this value is different from that ($n = 5$) in all other conditions. This difference is attributed to the difference in deformation mechanisms.

3.3. Strain Hardening Index and Strain Rate Sensitivity. Figure 6 shows the relationship between the strain hardening index (ϑ) and the test temperature. The value of ϑ was 1.25 to 1.6 at the test temperature of 523 K, and the effect of the strain rate is relatively small. However, ϑ decreased as the temperature increased, and the rate of decrease increased as the strain rate decreased. The decrease in the value of ϑ was larger under the conditions in which the stationary deformation behavior was observed from the nominal-stress-nominal-strain curve shown in Figure 3. Under the assumption that the stationary deformation occurred depending on the balance between dynamic recovery or recrystallization and work hardening, the decrease in ϑ at high temperatures and low strain rates may be attributed to dynamic recovery and recrystallization [37].

Figure 7 shows the relationship between the initial strain rate and the plastic flow stress. Here, we defined the plastic flow stress as the net stress that is involved in plastic deformation by subtracting the proof stress from the maximum stress. The relationship between the strain rate and the plastic flow stress at 523 K is represented by a gradual curve for which m is about 0.1, and the strain rate sensitivity was small. On the other hand, the relationship at 623 K is represented as a curve that bends as the strain rate decreases; the m value at low strain rates is approximately 0.3, and the strain rate sensitivity was high. At 573 K, which is the intermediate temperature, the relationship is represented by a gradual curve whose shape is similar to that at 523 K for high strain rates and similar to that at 623 K for low strain rates; the m

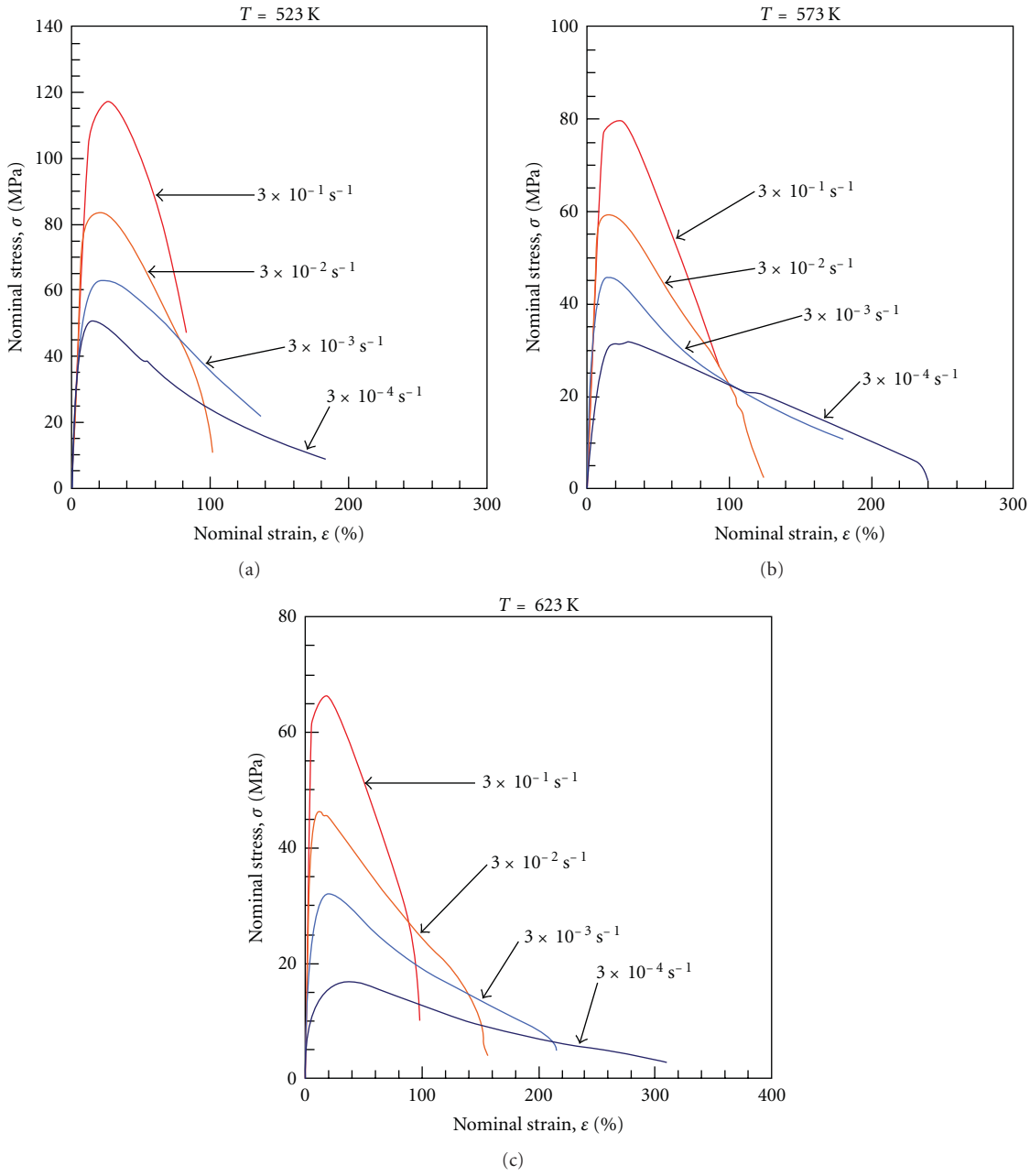

Figure 3: Nominal-stress-nominal-strain curves for tensile deformation at 523 K (a), 573 K (b), and 623 K (c) at an initial strain rate of 3×10^{-1} to 10^{-4} s^{-1}.

value for this curve is 0.2 and 0.3 for high and low strain rates, respectively.

3.4. Observation of Plate Surface Structure after High-Temperature Tensile Deformation. Figure 8 shows the deformed surface structure for the case in which the same degree of deformation was applied at each strain rate at 573 K and 623 K. The surface structure was observed by optical microscopy. On the basis of the results shown in Figures 5–7, we selected 573 K and 623 K as the test temperatures and 3.0×10^{-2} to 3.0×10^{-4} s^{-1} as the range of initial strain rates, which was believed to include the point at which the deformation transition occurred. To compare the structural change before breaking, we varied the degree of deformation according to the nominal stress-strain curve shown in Figure 3. Figure 8 shows that isometric cavities were formed as the strain rate decreased and the test temperature increased, while cavities that elongated in the tensile direction were formed at high strain rates. On the basis of the SEM structure (Figure 10) described later, the cavities were considered to grow and merge without elongation in the tensile direction because of active occurrence of grain boundary sliding (GBS) under high-temperature and low-strain-rate conditions. Since the structures observed by optical microscopy at 573 K and

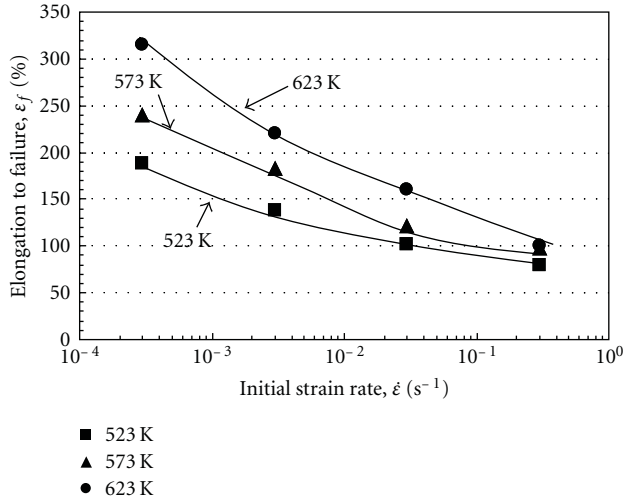

Figure 4: Relationship between elongation and initial strain rate of the AZ31 Mg rolled sheet. The test temperature is indicated in the figure.

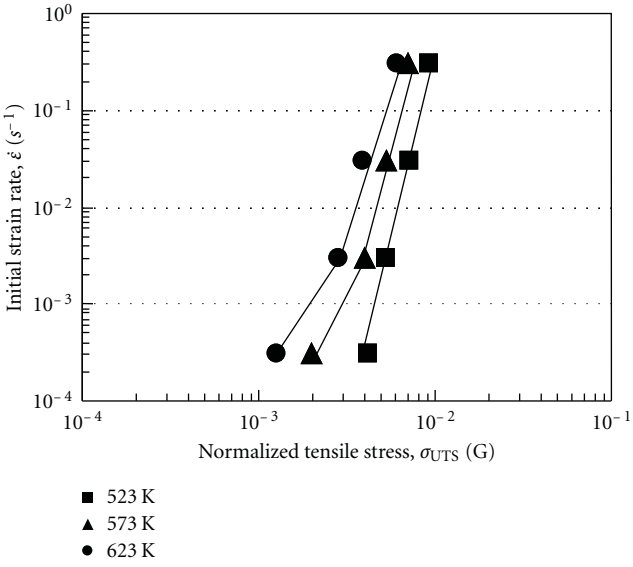

Figure 5: Relationship between the initial strain rate and tensile stress normalized by the shear modulus, for each test temperature.

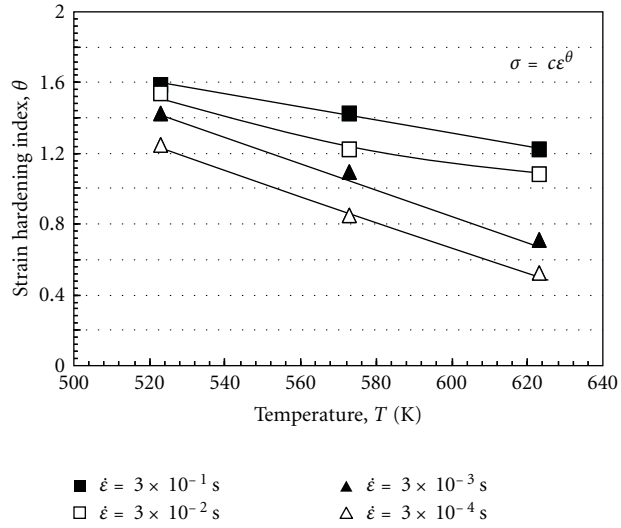

Figure 6: Relationship between the strain hardening ratio and test temperature.

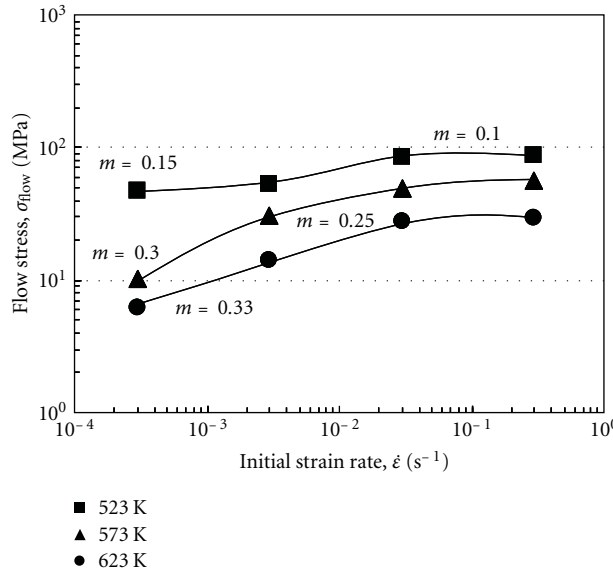

Figure 7: Relationship between the initial strain rate and plastic flow stress. The m value is indicated in the figure.

623 K were similar, we calculated the area fraction of cavities relative to the degree of deformation on the basis of these structures after causing deformation at 573 K and 623 K and initial strain rates of $3.0 \times 10^{-3}\,s^{-1}$ and $3.0 \times 10^{-4}\,s^{-1}$ (Figure 9). The area fraction of cavities relative to the degree of deformation increased as the test temperature increased and the strain rate decreased. At 573 K, the area fraction of cavities was proportional to the degree of deformation, while at 623 K, the relationship was proportional only until the degree of deformation reached 140% and the gradient of the area fraction of cavities varied with further deformation. To measure the area fraction of cavities while avoiding the effects of constriction, and so forth, which occur under a large deformation, we obtained measurements at a point 500 μm from the center of the parallel section. Figure 10 shows the SEM structures of the plate surface of the tensile specimen subjected to various degrees of deformation at 573 K and 673 K and an initial strain rate of $3.0 \times 10^{-3}\,s^{-1}$. At 573 K, GBS and transgranular sliding occurred and generated minute cavities on grain boundaries, although little unevenness was caused by GBS at 20% deformation. At 40% deformation, GBS was clearly dominant, and the surface of the tensile specimen was uneven. When the degree of deformation was 80% and higher, cavities were clearly observed and GBS occurred; further, a fiber-like structure [38, 39] was formed on the grain boundary, along with the growth of cavities. However, grains were not elongated in the tensile direction. At 673 K, unevenness

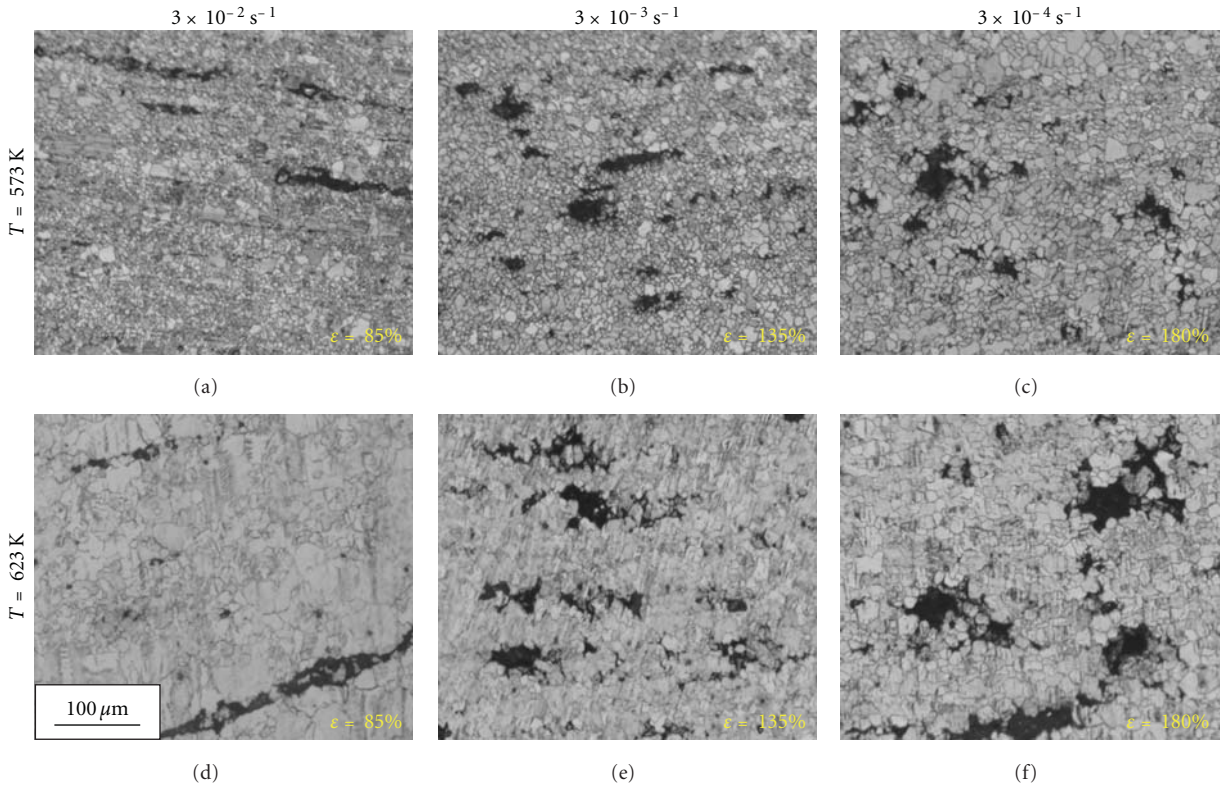

Figure 8: Optical micrographs of the as-rolled specimens deformed during tensile tests at 573 K (a)–(c) and 623 K (d)–(f), for $\varepsilon = 85\%$ (a, d), $\varepsilon = 135\%$ (b, e), and $\varepsilon = 180\%$ (c, f).

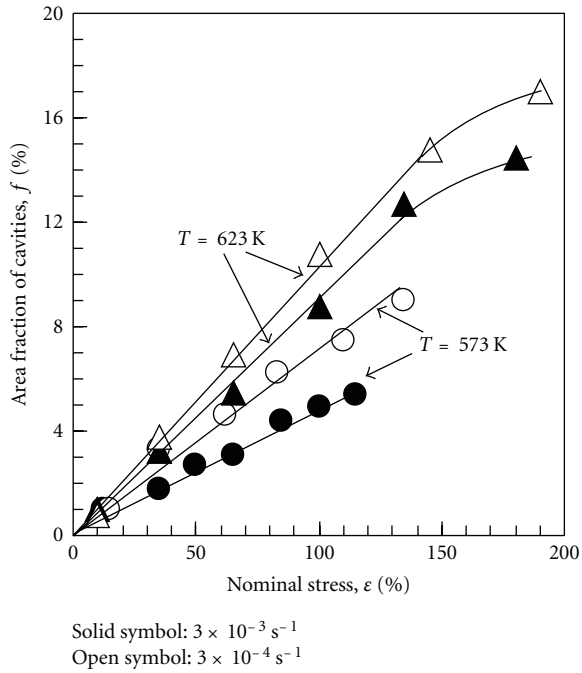

Figure 9: Relationship between the area fraction of cavities and nominal stress at 573 K and 623 K for each deformation ratio.

was clearly observed on the surface of the tensile specimen subjected to 20% deformation and a fiber-like structure and cavities formed on the grain boundary. It is surmised that the merging of cavities (Figure 10(g)) and transgranular sliding occurred as the degree of deformation was increased. Sliding deformation was more clearly observed at 623 K than at 573 K. Transgranular sliding was reported even for deformation temperatures of 573 K and above when the strain rate was low and the degree of deformation of the extruded AZ61 material was 30% [40]. The results of this study agree with this observation. The bending of the linear curve shown in Figure 5 at 573 K and 623 K and initial strain rates of 3.0×10^{-3} to 3.0×10^{-4} s^{-1}, as well as the large m value, are attributed to the fact that structural changes occurred mainly by GBS.

4. Discussion

4.1. Evaluation of the Stability of High-Temperature Deformation. On the basis of the experimental results, we found that the strength and breaking elongations of the AZ31 Mg alloy were dependent on the test temperature and strain rate at high temperatures; we also found that the mode of breaking changed from one involving constriction to one involving uniform elongation as the test temperature increased and the initial strain rate decreased. For stable and uniform deformation, the local deformation stress concurrent with work hardening should decrease and the constriction resistance (m value) should increase according to the local constriction deformation. However, the stability may vary depending on the constriction shape, even when the constriction is allowed to grow. To discuss the stability during deformation,

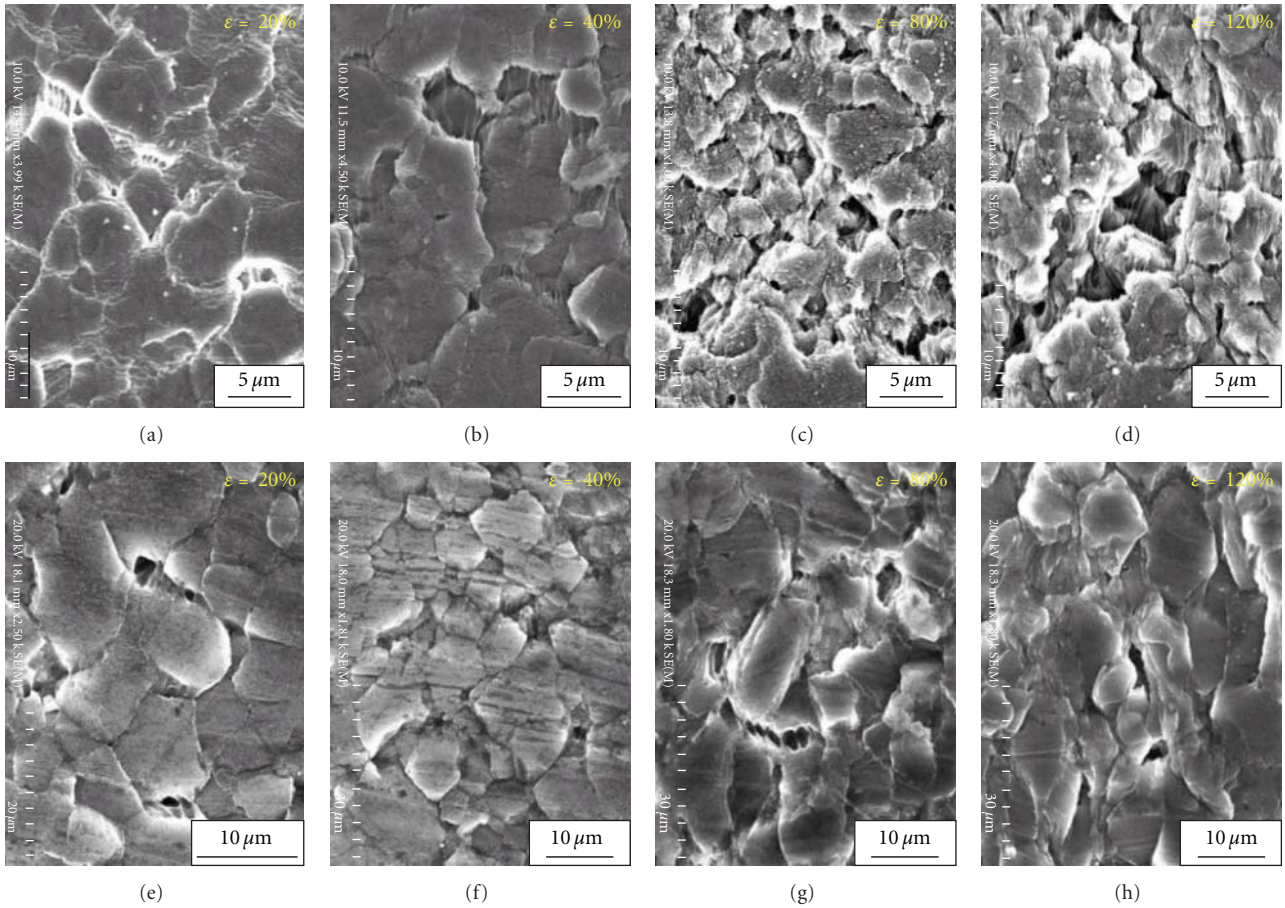

FIGURE 10: SEM micrographs of the as-rolled specimens deformed during tensile tests at 573 K (a)–(d) and 623 K (e)–(h) at an initial strain rate of $3 \times 10^{-3}\,s^{-1}$, for tensile deformation ratios of 20% (a, e), 40% (b, f), 80% (c, g), and 120% (d, h). The tensile direction is along the vertical direction.

parameters that indicate the changes in the shape of the constriction are required. Sato et al. [41] discussed such parameters and considered the deformation stability by introducing I in the following equation:

$$I(\varepsilon) = \frac{(\gamma - 1)}{m}. \tag{2}$$

Here, γ denotes the work hardening index and m denotes the strain rate sensitivity. According to the analysis by Sato et al. [41], constriction growth can be evaluated as follows: depending on I: constriction does not grow when $I > 0$, it grows slowly when $-1 < I < 0$, and it grows gradually from the beginning of deformation until it breaks; when $-2 < I$, the constriction grows sharply.

Therefore, we calculated $I(\varepsilon)$ by substituting for the work hardening index in (2), while setting ε to 0.1, 0.2, and 0.3 on the basis of the nominal stress-strain curve shown in Figure 3; further, we obtained the m value from Figure 7. The analytical results of the tensile test at 623 K are shown in Figure 11. $I(\varepsilon)$ decreases as the deformation increases, that is, as the work hardening decreases relative to the strain increment. Here, I decreases to -2 or less for strain rates of 3×10^{-1} to $10^{-2}\,s^{-1}$, while it is close to -2 at low strain rates of 3×10^{-3} to $10^{-4}\,s^{-1}$. For a similar analysis, I was close to -2 at 573 K ($3 \times 10^{-4}\,s^{-1}$) and -2 or less in all other cases. The results of this study show that to achieve stable deformation, the work hardening and constriction resistance must be balanced to cope with the large elongation; the results also show that the stability can be evaluated using $I(\varepsilon)$.

4.2. Transition of Deformation Mechanism. Figure 7 shows that the deformation mechanism for the test temperature of 573 K is represented by a gradual curve. The stress index under these conditions corresponded to the bending, and the test conditions (523 K and $3 \times 10^{-3}\,s^{-1}$) seemed to correspond to the point of transition of the deformation mechanisms. The high-temperature deformation map for pure Mg reported by Ashby and Verrall [42] indicates that the area that corresponds to the strength and temperature considered in this study seems to be the section where the deformation mechanism of the AZ31 Mg alloy shifts from plasticity to power-law creep. Although pure Mg and Mg alloys differ, a transition of the deformation mechanism is thought to occur for the AZ31 Mg alloy as well. Here, the structural observations reported by Noda et al. [43] indicate that the AZ31 Mg alloy is a fine-grain Al-Mg alloy but it

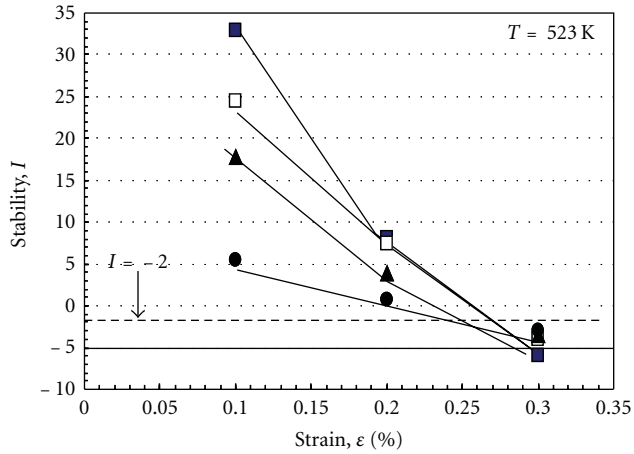

(a)

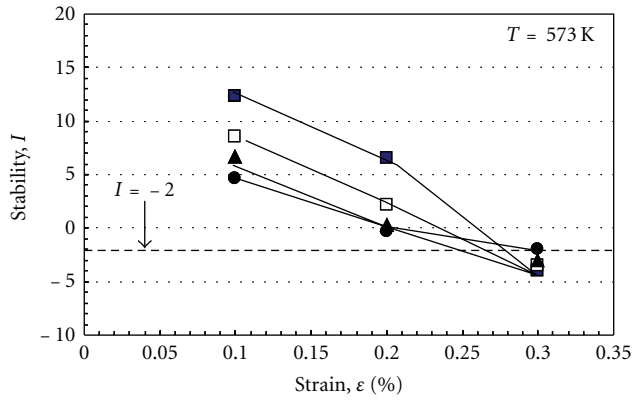

(b)

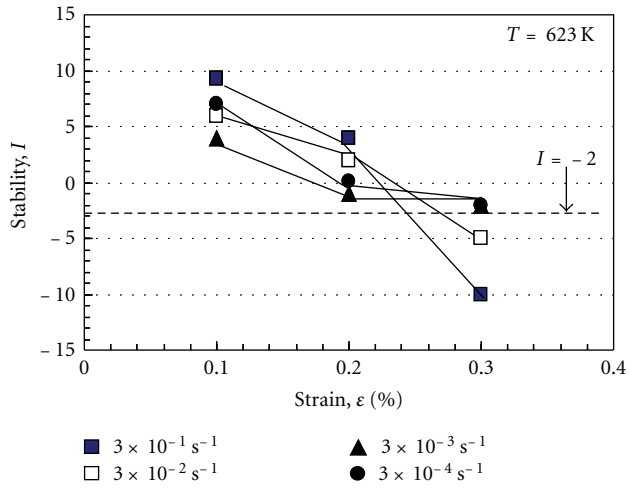

(c)

Figure 11: The dependence of the initial strain rate on neck stability (I), for several values of I calculated using (2); (a) 523 K, (b) 573 K, and (c) 623 K.

changes with the superplastic deformation mechanism at a test temperature of 473 K, owing to GBS and transgranular sliding. For initial grain sizes of 3 μm or less, a large elongation of over 200% can occur in the low-temperature range via transgranular sliding as the main deformation mechanism [34].

On the basis of structural observation, we assumed that the deformed section is the cause of the transition of the deformation mechanism. On the basis of the structural observations shown in Figure 10, as well as Figures 5–7 and 11, we assume that the deformation mechanism changes at 573 K and 3×10^{-3} s^{-1}. To study the deformation structure under these conditions, we performed SEM observation of the deformation structure after 40% deformation (Figure 12). Since we observed the projections of grain boundaries, the formation of the fiber structure on the grain boundaries, as well as minute cavities among the fiber structures, we assumed that GBS with concurrent formation of minute cavities was the main deformation mechanism [38, 39]. Figure 12(b) shows the observed deformation structure; crease-like patterns (indicated by arrows) were observed within the grains and transgranular sliding also occurred. Substructures are formed inside the grains of the material when it is deformed at a high rate and a low temperature [44]. The experimental results presented so far suggest that GBS is the main mechanism under low strain rates that result in stable deformation. For the AZ31 Mg alloy used in this study (grain size: ~5 μm), the change in the deformation mechanism at 523 K and 3×10^{-3} s^{-1} is attributed to (1) the change in the stable deformation behavior, (2) the change in the deformation mechanism to one dominated by GBS, and (3) the influence of the stability of the plastic deformation concurrent with GBS on the transition.

5. Conclusion

We conducted high-temperature tensile tests and evaluated the high-temperature deformation behavior and deformation mechanism of the AZ31 Mg alloy, to obtain basic data for developing plastic working technology. We obtained the following results.

(1) For the AZ31 Mg alloy, the high-temperature behavior mainly depends on the strain rate and deformation temperature. A stationary deformation area was observed, and a large elongation was evident as the temperature increased and strain rate decreased.

(2) The strain rate affects the work hardening and constriction resistance during high-temperature deformation. The stability of high-temperature deformation was evaluated by using the stability parameters $I(\varepsilon)$ obtained from the work hardening and constriction resistance; I was close to -2 for test conditions under which the large elongation occurred, and -2 or less under other test conditions. Therefore, I is an effective parameter for evaluating stability.

(3) The AZ31 Mg alloy used in this study had a grain size of approximately 5 μm. It is assumed that the

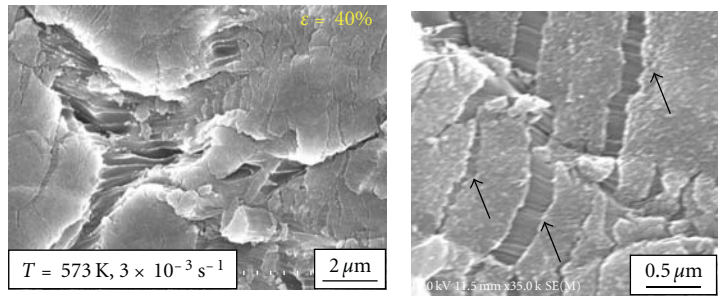

(a) (b)

FIGURE 12: The slip morphology on the specimen surface after 40% tensile deformation at a strain rate of 3×10^{-3} s^{-1} and a temperature of 573 K.

deformation mechanism changes beyond the test temperature of 523 K and the initial strain rate of 3×10^{-3} s^{-1} because of a change in the stable deformation behavior and transition in the deformation mechanism that is mainly dominated by GBS. It is also assumed that the transition is affected by the GBS concurrent with deformation.

Acknowledgment

This work was supported by the Advanced Machining Technology & Development Association (AMTDA).

References

[1] A. Tharumarajah and P. Koltun, "Is there an environmental advantage of using magnesium components for lightweighting cars?" *Journal of Cleaner Production*, vol. 15, no. 11-12, pp. 1007–1013, 2007.

[2] C. H. Caceres, "Economical and environmental factors in light alloys automotive applications," *Metallurgical and Materials Transactions A*, vol. 38, no. 7, pp. 1649–1662, 2007.

[3] J. Gediga and M. Betz, "Environmental benefits of new materials in automotive applications-LCE focusing on the recycling phase," *Journal of Advanced Science*, vol. 13, pp. 222–225, 2001.

[4] S. G. Pantelakis, N. D. Alexopoulos, and A. N. Chamos, "Mechanical performance evaluation of cast magnesium alloys for automotive and aeronautical applications," *Journal of Engineering Materials and Technology, Transactions of the ASME*, vol. 129, no. 3, pp. 422–430, 2007.

[5] C. R. Chakravorty, "Development of ultra light magnesium-lithium alloys," *Bulletin of Materials Science*, vol. 17, no. 6, pp. 733–745, 1994.

[6] H. Mori, M. Noda, and T. Tsujimura, "Feature view for application of advanced technology on metallic materials on technology for railway," *Railway Research Review*, vol. 62, pp. 26–29, 2005.

[7] B. L. Mordike and T. Ebert, "Magnesium properties—applications—potential," *Materials Science and Engineering A*, vol. 302, no. 1, pp. 37–45, 2001.

[8] F. Czerwinski, "Size evolution of the unmelted phase during injection molding of semisolid magnesium alloys," *Scripta Materialia*, vol. 48, no. 4, pp. 327–331, 2003.

[9] Y. Kawamura, K. Hayashi, A. Inoue, and T. Masumoto, "Rapidly solidified powder metallurgy MgZnY alloys with excellent tensile yield strength above 600 MPa," *Materials Transactions*, vol. 42, no. 7, pp. 1172–1176, 2001.

[10] Y. Chino, M. Kado, and M. Mabuchi, "Compressive deformation behavior at room temperature −773 K in Mg—0.2 mass%(0.035at.%)Ce alloy," *Acta Materialia*, vol. 56, no. 3, pp. 387–394, 2008.

[11] Y. Wang, S. B. Kang, and J. Cho, "Microstructural evolution of twin-roll cast Mg-3Al-0.5Mn-0.2Mm alloys during warm rolling and subsequent annealing," *Journal of Materials Processing Technology*, vol. 210, no. 10, pp. 1270–1275, 2010.

[12] C. Sanchez, G. Nussbaum, P. Azavant, and H. Octor, "Elevated temperature behaviour of rapidly solidified magnesium alloys containing rare earths," *Materials Science and Engineering A*, vol. 221, no. 1-2, pp. 48–57, 1996.

[13] S. Logan, "Magnesium technology 2007," in *The Minerals, Metals and Materials Society*, S. Randy et al., Ed., pp. 41–49, 2007.

[14] M. Noda, H. Mori, K. Funami, T. Tsujimura, and K. Higashi, "Screw processing by hot form rolling on magnesium alloy," *Journal of the Japan Society for Technology of Plasticity*, vol. 48, pp. 427–430, 2007.

[15] H. Yoshinaga and R. Horiuchi, "On the flow stress of α solid solution Mg-Li alloy single crystals," *Transactions of the Japan Institute of Metals*, vol. 4, pp. 134–141, 1963.

[16] A. Takara, Y. Nishikawa, H. Watanabe, H. Somekawa, T. Mukai, and K. Higashi, "New forming process of three-dimensionally shaped magnesium parts utilizing high-strain-rate superplasticity," *Materials Transactions*, vol. 45, no. 8, pp. 2531–2536, 2004.

[17] J. M. Boileau, P. A. Friedman, D. Q. Houston, and S. G. Luckey, "Superplastic response of continuously cast AZ31B magnesium sheet alloys," *Journal of Materials Engineering and Performance*, vol. 19, pp. 467–480, 2010.

[18] M. Liu, G. Yuan, Q. Wang, Y. Wei, W. Ding, and Y. Zhu, "Superplastic behavior and microstructural evolution in a commercial Mg-3Al-1Zn magnesium alloy," *Materials Transactions*, vol. 43, no. 10, pp. 2433–2436, 2002.

[19] R. Panicker, A. H. Chokshi, R. K. Mishra, R. Verma, and P. E. Krajewski, "Microstructural evolution and grain boundary sliding in a superplastic magnesium AZ31 alloy," *Acta Materialia*, vol. 57, no. 13, pp. 3683–3693, 2009.

[20] X. Zeng, Y. Zhang, C. Lu, W. Ding, Y. Wang, and Y. Zhu, "Precipitation behavior and mechanical properties of a Mg-Zn-Y-Zr alloy processed by thermo-mechanical treatment," *Journal of Alloys and Compounds*, vol. 395, no. 1-2, pp. 213–219, 2005.

[21] D. H. Bae, Y. Kim, and I. J. Kim, "Thermally stable quasicrystalline phase in a superplastic Mg-Zn-Y-Zr alloy," *Materials Letters*, vol. 60, no. 17-18, pp. 2190–2193, 2006.

[22] G. Yuan, Y. Liu, W. Ding, and C. Lu, "Effects of extrusion on the microstructure and mechanical properties of Mg-Zn-Gd alloy reinforced with quasicrystalline particles," *Materials Science and Engineering A*, vol. 474, no. 1-2, pp. 348–354, 2008.

[23] S. M. He, L. M. Peng, X. Q. Zeng, W. J. Ding, and Y. P. Zhu, "Comparison of the microstructure and mechanical properties of a ZK60 alloy with and without 1.3 wt.% gadolinium addition," *Materials Science and Engineering A*, vol. 433, no. 1-2, pp. 175–181, 2006.

[24] J. A. del Valle, F. Carreño, and O. A. Ruano, "On the threshold stress for superplasticity in Mg-Al-Zn alloys," *Scripta Materialia*, vol. 57, no. 9, pp. 829–832, 2007.

[25] F. K. Abu-Farha and M. K. Khraisheh, "Mechanical characteristics of superplastic deformation of AZ31Magnesium alloy," *Journal of Materials Engineering and Performance*, vol. 16, no. 2, pp. 192–199, 2007.

[26] H. Watanabe, A. Takara, H. Somekawa, T. Mukai, and K. Higashi, "Effect of texture on tensile properties at elevated temperatures in an AZ31 magnesium alloy," *Scripta Materialia*, vol. 52, no. 6, pp. 449–454, 2005.

[27] K. Kitazono, E. Sato, and K. Kuribayashi, "Internal stress superplasticity in polycrystalline AZ31 magnesium alloy," *Scripta Materialia*, vol. 44, no. 12, pp. 2695–2702, 2001.

[28] Y. Chino, M. Mabuchi, R. Kishihara et al., "Mechanical properties and press formability at room temperature of AZ31 Mg alloy processed by single roller drive rolling," *Materials Transactions*, vol. 43, no. 10, pp. 2554–2560, 2002.

[29] N. Srinivasan, Y. V. R. K. Prasad, and P. Rama Rao, "Hot deformation behaviour of Mg-3Al alloy-A study using processing map," *Materials Science and Engineering A*, vol. 476, no. 1-2, pp. 146–156, 2008.

[30] T. Mukai, H. Watanabe, and K. Higashi, "Application of superplasticity in commercial magnesium alloy for fabrication of structural components," *Materials Science and Technology*, vol. 16, no. 11-12, pp. 1314–1319, 2000.

[31] W. J. Kim, S. W. Chung, C. S. Chung, and D. Kum, "Superplasticity in thin magnesium alloy sheets and deformation mechanism maps for magnesium alloys at elevated temperatures," *Acta Materialia*, vol. 49, no. 16, pp. 3337–3345, 2001.

[32] X. Liu, R. Chen, and E. Han, "High temperature deformations of Mg-Y-Nd alloys fabricated by different routes," *Materials Science and Engineering A*, vol. 497, no. 1-2, pp. 326–332, 2008.

[33] X. Yang, Z. X. Ming, D. Y. Lai, and F. X. Hui, "Superplasticity of Mg-Gd-Y alloy in tensile test at elevated temperature," *Transactions of Nonferrous Metals Society of China*, vol. 17, pp. s372–s375, 2007.

[34] M. Noda, K. Funami, M. Hirohashi, and M. Kobayashi, "Effect of grain size and microstructure on appearance of low temperature superplasticity in Al-Mg alloy," *Materials Science Forum*, vol. 447-448, pp. 435–440, 2004.

[35] S. Goto, K. Mori, and H. Yosinaga, "Effect of particle shape on the high temperature yield strength of dispersion—hardened nickel base alloys," *Journal of the Japan Institute of Metals*, vol. 50, pp. 154–161, 1986.

[36] S. P. Bhat and C. Laird, "High temperature cyclic deformation of nickel," *Fatigue of Engineering Materials and Structures*, vol. 1, pp. 59–77, 1979.

[37] H. Y. Wu and F. Z. Lin, "Mechanical properties and strain-hardening behavior of Mg alloy AZ31B-H24 thin sheet," *Materials Science and Engineering A*, vol. 527, no. 4-5, pp. 1194–1199, 2010.

[38] Q. Yang and A. K. Ghosh, "Formability of ultrafine-grain Mg Alloy AZ31B at warm temperatures," *Metallurgical and Materials Transactions A*, vol. 39, no. 11, pp. 2781–2796, 2008.

[39] M. G. Zelin, "On micro-superplasticity," *Acta Materialia*, vol. 45, no. 9, pp. 3533–3542, 1997.

[40] Y. N. Wang and J. C. Hung, "Transaction of dominant diffusion process during superplastic deformation in AZ61 magnesium alloys," *Metallurgical and Materials Transactions A*, vol. 35, pp. 555–562, 2004.

[41] E. Sato, K. Kuribayashi, and R. Horiuchi, "Study on plastic instability in superplastic deformation through analysis of the neck shape change," *Journal of the Japan Institute of Metals*, vol. 52, no. 11, pp. 1051–1056, 1988.

[42] M. F. Ashby and R. A. Verrall, "Diffusion-accommodated flow and superplasticity," *Acta Metallurgica*, vol. 21, no. 2, pp. 149–163, 1973.

[43] M. Noda, M. Hirohashi, and K. Funami, "Low temperature superplasticity and its deformation mechanism in grain refinement of Al-Mg alloy by multi-axial alternative forging," *Materials Transactions*, vol. 44, no. 11, pp. 2288–2297, 2003.

[44] M. M. Myshlyaev, H. J. McQueen, A. Mwembela, and E. Konopleva, "Twinning, dynamic recovery and recrystallization in hot worked Mg-Al-Zn alloy," *Materials Science and Engineering A*, vol. 337, no. 1-2, pp. 121–133, 2002.

Hindawi Publishing Corporation
Journal of Metallurgy
Volume 2011, Article ID 924032, 5 pages
doi:10.1155/2011/924032

Research Article

α'' Martensitic Twinning in Alpha + Beta Ti-3.5Al-4.5Mo Titanium Alloy

Changfu Li,[1] Geping Li,[1] Yi Yang,[2] Mesut Varlioglu,[3] and Ke Yang[1]

[1] *Institute of Metal Research, Chinese Academy of Sciences, 72 Wenhua Road, Shenyang 110016, China*
[2] *Northwest Institute For Non-Ferrous Metal Research, 96 Weiyang Road, Xi'an 710016, China*
[3] *Cobham Mission Systems Division, 2734 Hickory Grove Road, Davenport, IA 52804, USA*

Correspondence should be addressed to Geping Li, gpli@imr.ac.cn

Received 30 December 2010; Accepted 7 April 2011

Academic Editor: Chong Soo Lee

The twinning structure of the orthorhombic α'' martensite phase in alpha + beta Ti-3.5Al-4.5Mo (wt%) titanium alloy was studied using X-ray diffraction and transmission electron microscopy by water quenching from below transus temperatures. While water quenching from 910°C induced the formation of $\{110\}_{\alpha}$ twins, quenching from 840°C formed the α'' martensite with $\{111\}_{\alpha}$ type I twins. The effect of the principle strains on the twinning structure was discussed. As compared to the previous studies, the principle strains play an important role in the formation of the twinning type.

1. Introduction

Commercial $\alpha + \beta$ titanium alloys are widely used in structural and aerospace applications where the combination of light weight, strength, and room temperature corrosion resistance is highly desired. With different alloy compositions and thermomechanical processing parameters, a wide range of mechanical properties can be achieved in titanium alloys. Beside the enhanced mechanical properties, metastable martensite microstructure can be obtained with fast cooling from body-centered cubic (bcc) β phase region. While near alpha titanium alloys yield only small fraction of martensite structure, alpha + beta titanium alloys can produce a combination of hcp (α') and c-orthorhombic (α'') martensite phase [1, 2]. α'' phase is particularly interesting because it can be thermoelastic, and better understanding of this phase transformation can be used to design smart systems.

There have been extensive studies on the properties of α' [3–6] and the phenomenological theory martensite crystallography (PTMC) [7, 8]. Unlike the α' martensite transformation, the α'' martensite transformation which was first found in a Ti-Nb system [9] can be thermoelastic, and the shape memory effect is present [10–14]. The crystal structure of α'' martensite is intermediate between bcc β and hcp α phases [9], and the lattice parameters vary with alloy compositions significantly [15]. The morphology of α'' martensite depends on the magnitude of the lattice deformation. It was found in Ti-Ta alloy that most of the α'' martensite are not twinned state at a certain Ta content [16], while most literatures concerning the α'' martensite twin structure in β titanium alloys reported that the α'' martensite is in $\{111\}$ twin structure [17, 18]. However, the morphology and crystallography of α'' martensite twin has not been completely described, especially for the $\alpha + \beta$ titanium alloys in which the β isomorphic elements are very close to the lower critical concentration of α'' martensite.

It is well known that twinning is a deformation process of most engineering materials to reduce the overall energy of the system, thus, the determination of twinning structure of the orthorhombic α'' martensite is essential for better understanding of the deformation mechanism and future development of titanium alloys. In this study, we have investigated an $\alpha + \beta$ titanium alloy with nominal composition of Ti-3.5Al-4.5Mo (wt%). This alloy is based on Russian Ti-4.5Al-3Mo-1V (VT14) high-strength titanium alloy mainly used for stampings, gear applications [19]. By reducing the aluminum and omitting vanadium contents, we

have reduced the amount of β phase so that the martensite microstructure would contain no retained β phase and the identification of α'' phase would be more pronounced. Considering the β transus temperature of this alloy is about 925°C where the cubic β phase can transform to hexagonal α phase, we have selected 910°C and 840°C as quenching temperatures where they refer to the highest temperature that α'' phase can be observed and the lowest temperature that the microstructure will be mostly α'' phase after water quenching, respectively.

2. Experimental Procedure

A titanium alloy ingot with 60 gr weight was prepared in a nonconsumable arc melting furnace under protective argon atmosphere. The ingot was homogenized at 1200°C for 2 hours followed by air cooling and then forged at 900°C to a bar shape with $10 \times 10 \times 130\,\text{mm}^3$ dimensions. The Energy Dispersive Spectroscopy (EDS) analysis showed that the composition of the ingot is Ti-3.63Al-4.41Mo (wt%). Two samples with $10 \times 10 \times 10\,\text{mm}^3$ cube shape were cut from the bar and heat-treated at 910°C or 840°C for 1 h followed by water quenching. The α'' martensite transformation depends on the quenching rate and alloy composition [20, 21]. In present study, the samples were used in identical dimensions so that the quenching rate effect in different samples will be insignificant. Phase distributions and lattice parameters were measured with the Rigaku D/max-2400PC X-Ray diffractometer using Cu-K_α radiation at 56 kV voltage and 182 mA current. The microstructures from each quenching temperatures were analyzed with the Technai $G^2$20 transmission electron microscope operating at 200 kV. TEM foils were mechanically thinned to about 30 μm in thickness, and further reduction was carried out using MTP-1A magnetic force-driven twin-jet electrolytic polisher in a solution of 20% perchloric acid, 30% butyl alcohol, and 50% methanol (vol.%) at −30°C to −40°C and a current of 15–20 mA.

3. Results and Discussions

The lattice parameters of samples quenched from 840°C or 910°C were calculated from the corresponding X-ray diffraction patterns shown in Figure 1. The lattice parameters consistently changed as compared to previous studies [15]. The lattice parameters of α'' martensite phase were calculated as $a_0 = 0.3120$ nm, $b_0 = 0.4990$ nm, and $c_0 = 0.4670$ nm after quenched from 910°C and $a_0 = 0.3130$ nm, $b_0 = 0.4920$ nm, and $c_0 = 0.4640$ nm after quenched from 840°C, respectively. The average errors to calculate the lattices parameters were ±0.001 nm. According to the principle of phase equilibrium, the isomorphic β-stable elements (M_0 in present alloy) in the β phase are richer when solution treated at 840°C than that at 910°C. Thus, a_0 in the unit cell increases while b_0 and c_0 decrease. Such lattice distortion due to different quenching temperatures was induced by the enriched molybdenum content in the β phase and α'' phase.

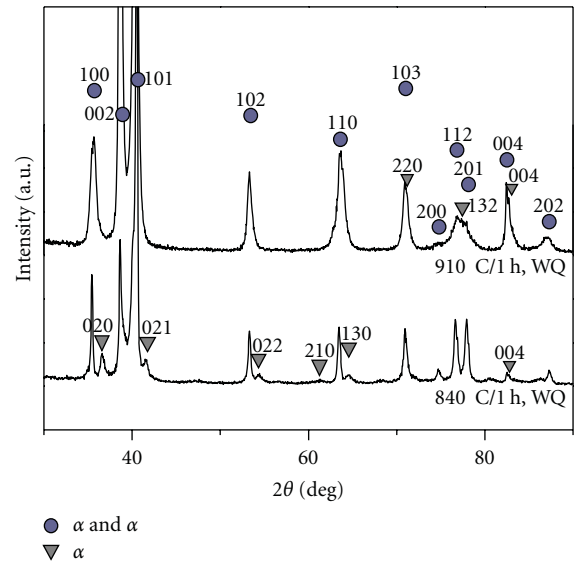

Figure 1: The X-ray diffraction patterns of the samples quenched from 840°C or 910°C. Marked α, α', and α'' phases are the hexagonal, hexagonal martensite, and orthorhombic martensite structures, respectively.

The phase transformation between the β and α'' martensite phase can be explained with Au-Cd-type transformation [22], as shown in Figure 2 where cubic β transforms to orthrhombic α'' martensite phase. The twinning relationships can be generally categorized into two classes. Inamura [20] named these classes as "class A" transformation for $\{111\}_0$ type I twinning and "class B" transformation for $\{011\}_0$ compound twinning. The twinning planes for class A and B were expressed as $\{011\}_\beta$ and $\{100\}_\beta$, respectively.

Figure 3(a) shows the TEM bright field image of the sample quenched from 910°C, and Figure 3(b) shows the corresponding selected area electron diffraction (SAED) pattern taken from the marked area. The α'' martensite twins locate between α' laths and is (011) twinning, that is, "class B". Most of the twins in the α'' martensite were in "class B" type, and the "class A" type twinning was rarely observed. Figures 3(c) and 3(d) show the TEM bright field image of the sample quenched from 840°C, and the SAED pattern taken from the encircled area in (c), respectively. The α'' martensite distributes between the remnant β phase laths. The "class A" transformation, namely, the $\{111\}_0$ type I twinning was confirmed by the Figure 3(d). In contrast with sample quenched from 910°C, the α'' martensite in the sample quenched from 840°C is almost in "class A" and the "class B" transformation was rarely observed.

As shown in Figure 1, the β phase transformed to $\alpha' + \alpha''$ and $\alpha'' + \beta$ phases due to the isomorphic β stable elements after water quenched from 910°C and 840°C, respectively. The Burgers orientation relationship (OR) between β and α' is $\{0001\}_\alpha // \{110\}_\beta$ and $\langle 1120\rangle_\alpha // \langle 110\rangle_\beta$, the OR of β and α'' is $\{001\}_{\alpha''} // \{110\}_\beta$ and $\langle 100\rangle_{\alpha''} // \langle 001\rangle_\beta$ [15]. When the partial β phase transforms into a set of parallel α' laths during quenching, the $(011)_\beta$ twin plane extends along

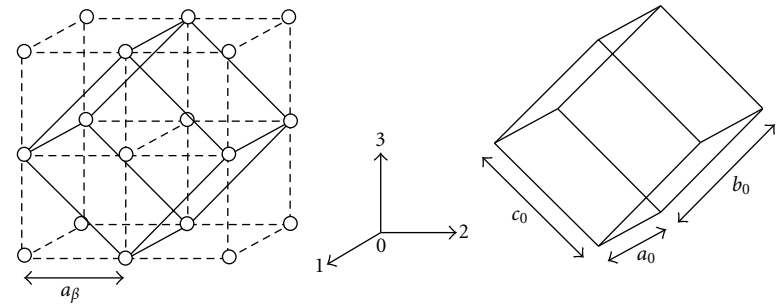

Figure 2: The schematic Au-Cd-type lattice phase transformation. Cubic β phase (left) with a_β lattice parameter transforms to α'' martensite (right) with a_0, b_0, and c_0 lattice parameters.

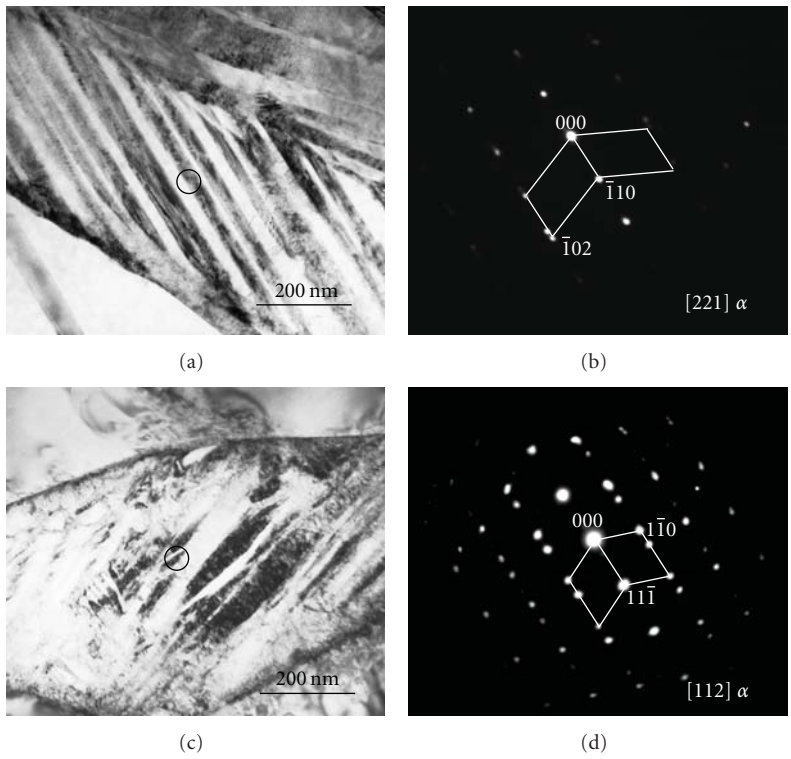

Figure 3: (a) The TEM bright field image of the sample quenched from 910°C, (b) the corresponding SAED pattern of the encircled area obtained from sample quenched from 910°C, the α'' martensite is in the class B transformation, namely, the $\{110\}_0$ compound twinning. (c) A representative TEM bright field micrograph structure in the sample quenched from 840°C and the SAED pattern from the circled region is shown in (d); and the α'' martensite is $\{111\}_0$ type I twinning, belonging to class A transformation.

the $[011]_\beta$ direction with a formation of residual stress. If the α'' martensite twin phase nucleates in this region, the newly formed twins will form by making 45° with the habit plane as the preferred slide plane will make a maximum Schmidt factor. By referring to Figure 2, the possible slide plane is $\{100\}_\beta$. When the product of $\alpha'' + \beta$ is obtained during quenching, the remnant β phase shrinks and compressive stress is developed. While the remnant β phase shrinks, newly formed α'' phase will develop and tensile stresses appear along $\{001\}$ direction families to reduce the overall energy of the system. The discussion about the elastic strain energy reduction follows in the next section.

During the twin formation of the α'' martensite, the elastic strain energy is significantly high due to variations in the free energy of the system. Mura [23] used the Eshelby's model to estimate the elastic strain energy per unit volume, W, of a thin plate parallel to $(hkk)_\beta$ for isotropic media as

$$W = \frac{\mu}{1-\nu}\left[\left(\frac{B}{A}\eta_2 + \eta_3\right)^2 - 2\frac{B}{A}(1-\nu)\eta_2\eta_3\right], \quad (1)$$

where $A = h^2 + 2k^2$ and $B = h^2 - 2k^2$, $\eta_1 = (a_0 - a_\beta)/a_\beta, \eta_2 = (b_0 - \sqrt{2}a_\beta)/\sqrt{2}a_\beta$, $\eta_3 = (c_0 - \sqrt{2}a_\beta)/\sqrt{2}a_\beta$ are the magnitude of the principle strain components of the $\beta - \alpha''$ martensite

transformation [20], and μ and ν are the shear modulus and Poisson's ratio, respectively. The lattice parameter of the β phase was taken as 0.330 nm when η_2 and η_3 were calculated by using the lattice parameters measured from the samples quenched at different temperatures. By using the formula above, the elastic strain energies were calculated per unit volume of the α'' martensite thin plate parallel to $\{011\}_\beta$ and $\{100\}_\beta$, respectively. It was found that $W\{100\}_\beta$ becomes much larger than $W\{011\}_\beta$ when η_3 is a tensile strain at 910°C, and $W\{100\}_\beta$ is much smaller than $W\{011\}_\beta$ when η_3 is a compressive strain at 840°C.

In the process of $\beta - \alpha''$ martensite transformation, one unit cell of the α'' martensite corresponds to two unit cells of the β phase, the volume of a unit cell of α'', V_0, is $a_0 \times b_0 \times c_0$, and the volume of two unit cells, V_β, is $2 \times a_\beta \times a_\beta \times a_\beta$. V_O is about 1.2% larger than V_β in the sample quenched from 910°C, while V_O is about 1.0% smaller than V_β in the sample quenched from 840°C. When the local twin structure expands, the higher magnitude of the elastic strain energy would decrease the free energy in the α'' martensite due to increased molybdenum content. In shrinking regions, a lower free energy state can be obtained with larger magnitude of W. Thus, $W\{100\}_\beta$ is thermodynamically favorable when the sample is quenched from 910°C. When the local twin structure shrinks, the elastic strain energy would be positive, a larger W can also make a lower energy condition, and $W\{011\}_\beta$ is thermodynamically favorable when the sample is quenched from 840°C.

Different W may introduce different twinning systems into the alloys. As described before that the main twinning system of α'' martensite in the sample quenched from 910°C is class B, while class A in the sample quenched from 840°C. This yields to a conclusion that low isomorphic β-stable elements can introduce a high strain in the water quenched microstructure, and $\{011\}_0$ compound twinning is likely to form. $\{111\}_0$ type I twinning is preferred in a water quenched microstructure with high β-stable elements. In fact, most of the observed α'' martensite twin structure in β titanium alloys are $\{111\}_0$ twin structure [17, 18].

It is also important to note that not all research finds the $\{111\}_0$ compound twinning as the predominant twin structures in β titanium alloys. Based on the theory of deformation twinning given by Bilby and Crocker, Ping [21], the possible deformation twinning is mainly $\{110\}_0$ compound twinning in β-Ti alloys, and the result was confirmed by his investigation. This would be another proof that the strain induces the formation of $\{110\}_0$ twinning when principle strain η_3 is plus. Similarly, increased content of the isomorphic β-stable elements distorts the lattice with a negative η_3 and promotes the formation of the $\{111\}_0$ type I twinning. The results from both quenching temperatures consistently show these twin structures.

4. Conclusions

The orthorhombic α'' martensite twinning was investigated in the Ti-3.5Al-4.5Mo (wt%) alloy. Quenching from 910°C induced the formation of $\{110\}_0$ compound twinning, while the α'' martensite is mainly the $\{111\}_0$ type I twinning in the sample quenched from 840°C. The type of α'' martensite twin structure is highly dependent on the principle strain, that is, a tensile η_3 leads to form $\{110\}_0$ twinning while a compressive η_3 induces the formation of the $\{111\}_0$ type I twinning. The contents of the isomorphic β-stable elements in the titanium alloy is the main effect on the formation of the principle strains and determines the type of α'' martensite twin structure.

Acknowledgment

The authors wish to thank Institute of Metal Research staff for the help in the TEM and X-ray diffraction measurements.

References

[1] G. Lutjering and J. C. Williams, *Titanium*, Springer, Berlin, Germany, 2003.

[2] M. Yotara, I. Osamu, and N. Takashi, in *Titanium Science and Technology*, G. Lutjering, U. Zwicker, W. Bunk, and D. G. M. Oberusel, Eds., p. 1403, FRG, 1985.

[3] P. Gaunt and J. W. Christian, "The crystallography of the β-α transformation in zirconium and in two titanium-molybdenum alloys," *Acta Metallurgica*, vol. 7, no. 8, pp. 534–543, 1959.

[4] A. V. Dobromyslov and V. A. Elkin, "Martensitic transformation and metastable β-phase in binary titanium alloys with d-metals of 4-6 periods," *Scripta Materialia*, vol. 44, no. 6, pp. 905–910, 2001.

[5] K. M. Knowles and D. A. Smith, "The nature of the parent-martensite interface in titanium-manganese," *Acta Metallurgica*, vol. 29, no. 8, pp. 1445–1466, 1981.

[6] Y. Ohmori, T. Ogo, and K. Nakai, "Effects of w-phase Precipitation on $\beta \rightarrow \alpha, \alpha''$ Transformations in a Meta-stable β Titanium Alloy," *Materials Science and Engineering A*, vol. 182, p. 312, 2001.

[7] J. S. Bowles and J. K. Mackenzie, "The crystallography of martensite transformations I," *Acta Metallurgica*, vol. 2, no. 1, pp. 129–137, 1954.

[8] M. S. Wechsler, D. S. Lieberman, and T. A. Read, "On the theory of the formation of martensite," *Journal of Metals*, vol. 197, pp. 1503–1515, 1953.

[9] A. R. G. Brown and K. S. Jepson, *Memoires et Etudes Scientifiques de la Revue de Metallurgie*, vol. 36, 1966.

[10] C. Baker, "The Shape-memory Effect in a Titanium-35wt%Niobium Alloy," *Metal Science Journal*, vol. 5, p. 92, 1971.

[11] Y. L. Hao, S. J. Li, B. B. Sun, M. L. Sui, and R. Yang, "Ductile Titanium Alloy with Low Poisson's Ratio," *Physical Review Letters*, vol. 98, Article ID 216405, 2007.

[12] M. Niinomi, "Recent Metallic Materials for Biomedical Applications," *Metallurgical and Materials Transactions A*, vol. 33, p. 477, 2002.

[13] T. W. Duerig, J. Albrecht, D. Richter, and P. Fischer, "Formation and reversion of stress induced martensite in Ti-10V-2Fe-3Al," *Acta Metallurgica*, vol. 30, no. 12, pp. 2161–2172, 1982.

[14] T. Saito, T. Furuta, J. H. Hwang et al., "Multifunctional alloys obtained via a dislocation-free plastic deformation mechanism," *Science*, vol. 300, no. 5618, pp. 464–467, 2003.

[15] K. K. Kharia and H. J. Rack, "Martensitic Phase Transformations IMI550(Ti-4Al-4Mo-2Sn-0.5Si)," *Metallurgical and Materials Transactions A*, vol. 32, p. 1671, 2001.

[16] K. A. Bywater and J. W. Christian, "Martensitic Transformations in Titanium-Tantalum Alloys," *Philosophical Magazine*, vol. 25, p. 1249, 1972.

[17] Y. Mantani, Y. Takemoto, A. Sakakibara, and M. Tajima, "Phase transformation of α'' martensite structure by aging in Ti-8mass%Mo alloy," *Materials Transactions*, vol. 45, no. 5, pp. 1629–1634, 2004.

[18] Y. W. Chai, H. Y. Kim, H. Hosoda, and S. Miyazaki, "Interfacial defects in Ti-Nb shape memory alloys," *Acta Materialia*, vol. 56, no. 13, pp. 3088–3097, 2008.

[19] E. N. Novikova, S. I. Gurevich, and L. M. Nikitina, "Nitriding of the VT14 alloy for gears," *Metal Science and Heat Treatment*, vol. 7, no. 10, pp. 639–642, 1965.

[20] T. Inamura, J. I. Kim, H. Y. Kim, H. Hosoda, K. Wakashima, and S. Miyazaki, "Composition dependent crystallography of α''-martensite in Ti-Nb-based β-titanium alloy," *Philosophical Magazine*, vol. 87, no. 23, pp. 3325–3350, 2007.

[21] D. H. Ping, Y. Yamabe-Mitarai, C. Y. Cui, F. X. Yin, and M. A. Choudhry, " Stress-induced α'' martensitic (110) twinning in β-Ti alloys," *Applied Physics Letters*, vol. 93, no. 15, Article ID 151911, 2008.

[22] D. S. Lieberman, M. S. Wechsler, and T. A. Read, "Cubic to orthorhombic diffusionless phase change—experimental and theoretical studies of AuCd," *Journal of Applied Physics*, vol. 26, no. 4, pp. 473–484, 1955.

[23] T. Mura, *Micromechanics of Defects in Solids*, Kluwer, Dordrecht,The Netherlands, 1987.

Hindawi Publishing Corporation
Journal of Metallurgy
Volume 2011, Article ID 747198, 5 pages
doi:10.1155/2011/747198

Research Article

A Study of the Quench Sensitivity of 6061-T6 and 6069-T6 Aluminum Alloys

M. E. Kassner,[1] P. Geantil,[2] and X. Li[2]

[1] *Department of Aerospace and Mechanical Engineering, University of Southern California, Los Angeles, CA 90089, USA*
[2] *LSI Logic, Gresham, OR 97006, USA*

Correspondence should be addressed to M. E. Kassner, kassner@usc.edu

Received 28 August 2010; Accepted 23 March 2011

Academic Editor: Chong Soo Lee

The purpose of this study is to investigate the quench sensitivity of the mechanical properties of 6061 and 6069 aluminum alloys. The relationship between mechanical properties and quench delay time at various temperatures between 200–500°C was determined. It was concluded that the 6069-T6 was somewhat more quench sensitive than 6061, which may be consistent with the composition difference. This study also provides increased data on the quench sensitivity of the traditional alloy, 6061-T6.

1. Introduction

The mechanical properties of the relatively new 6xxx series alloy, 6069, were extensively discussed by the authors in [1–3]. The objective of this study was to determine the quench sensitivity of the new alloy 6069, especially as compared to the traditional 6061 alloy. That is, on rapidly cooling from the solution annealing temperature by quenching, any reduction in the cooling rate translates to longer times at intermediate temperatures where "uncontrolled" nucleation can occur and lead to lower T6 properties subsequent to aging. The mechanical properties response varies for a given, decreased, cooling rate depending on the alloy composition. Gullotti et al. [4] and others [5, 6] found that for the 6xxx alloys, those that had higher Mg, Si, Mn, Cr, and Zr were more likely to have relatively accelerated Mg_2Si precipitation leading to diminished T6 mechanical properties. Mondolfo [7] reported that Cu increases quench sensitivity, but Zoller et al. [5] found that Cu actually alleviates quench sensitivity somewhat. The alloy 6069 has been demonstrated to have superior T6 fatigue, tensile, and fracture toughness properties over 6061 [1, 2]. However, the improved properties are provided in association with alloy additions Mg, Si, Cr (and Cu for which the effect is uncertain) which may render 6069 more quench sensitive. Thus, this investigation assessed the quench sensitivity of 6061 and 6069, both prepared identically from extruded air slip direct chill casting (Air-Slipor'ASDC). Both were solution treated at the same temperature and "quenched" into salt baths at various temperatures for various times followed by a water quench. The times at temperatures for a fixed deterioration (e.g., 5%) of T6 tensile (yield stress and ultimate tensile stress) were determined.

2. Experimental Methods

The 6061 and 6069 aluminum alloys used in this study were extruded at Anodizing Inc. (Portland, Ore) from Air-Slip Direct Chill Cast (ASDC) ingots provided by Northwest Aluminum Company. 6061 ingot was extruded into solid flat bar with a thickness of 9.53 mm and width of 38.1 mm. 6069 (228.6 mm diameter) ingot was extruded into solid round bar of 38.1 mm in diameter. The 6061 and 6069 ingots were pre heat treated before extrusion. The compositions of 6061 and 6069 aluminum alloys used in this study as well as 6061 sheet of an earlier (comparison) study from [4] are listed in Table 1.

The tensile specimens of 6061 and 6069 aluminum alloys of this study were cut along the extrusion direction and machined into round specimens with 2.54 mm diameter and 10.2 mm gage length. The specimens were solution heat-treated at 566°C for 1.5 hours with an accuracy of 1.5°C.

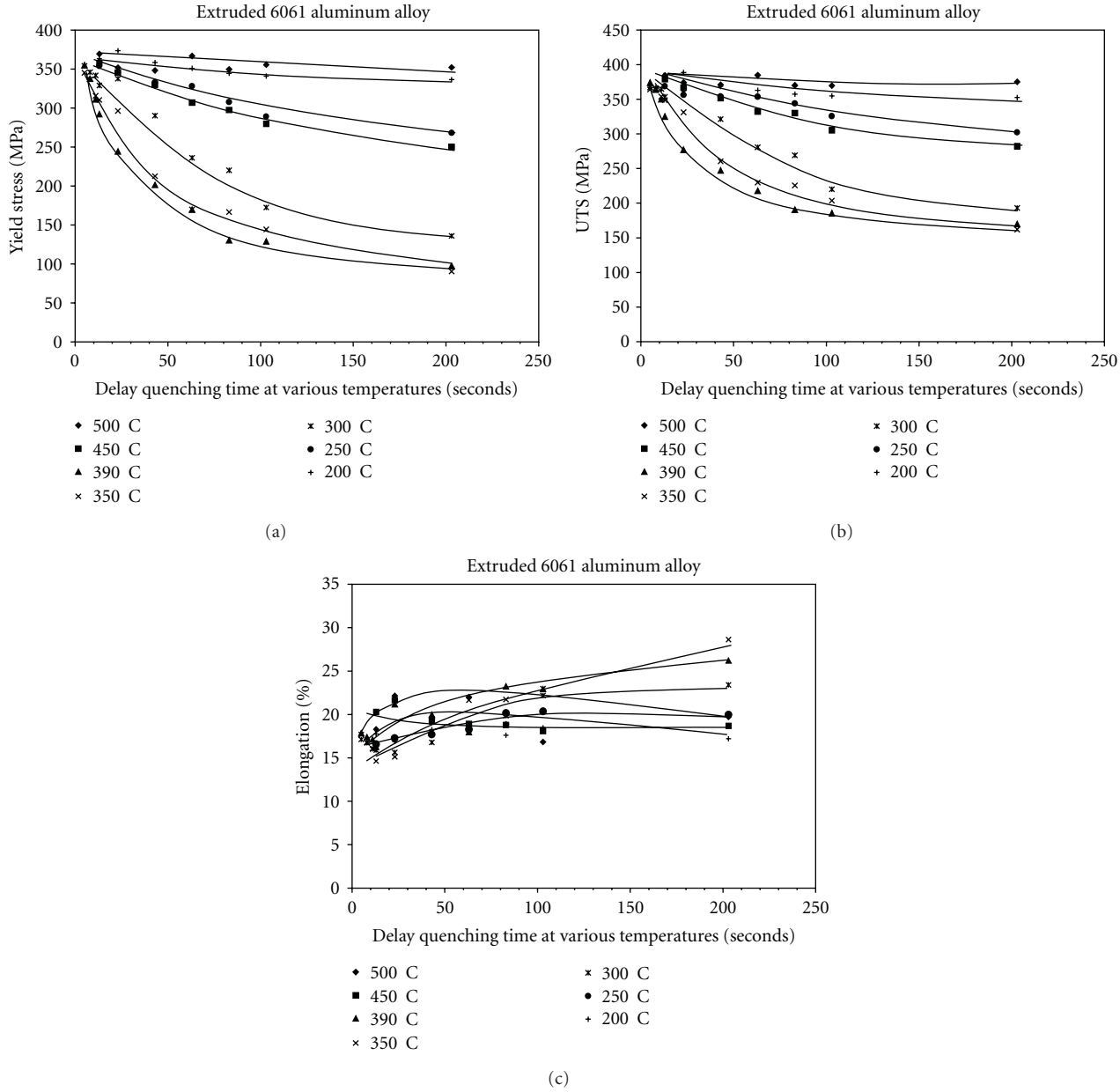

Figure 1: The effect of delayed quenching on the 6061-T6 (a) yield strength, (b) UTS, and (c) elongation.

Table 1: The composition of extruded 6061 and 6069 alloys used in this study as well as 6061 sheet [4].

	Composition, %wt.									
	Si	Fe	Cu	Mn	Mg	Cr	Ti	V	Ga	Zn
6061 (this study)	0.65	0.23	0.23	0.02	0.89	0.06	0.024	0.01	0.01	—
6069 (this study)	0.88	0.30	0.71	—	1.4	0.22	0.032	0.01	0.02	0.01
6061 (from [4])	0.66	0.38	0.23	0.12	0.98	0.12	0.014	—	—	0.07

The specimens were then quenched into a molten salt bath at various temperatures (200–500°C) for various times (3–200 seconds) and then water quenched to ambient tem-perature. The (molar) composition of molten salt used in the temperature range of 300 to 500°C was 18.3% KCl, 50.4% LiCl, 8% NaCl, and 23.3% RbCl. The (molar) composition of molten salt used in the temperature range of 200 to 300°C was 56% $AlCl_3$, 7% KCl, and 37% LiCl. Thermocouples were placed inside the center of a "control" specimen, and the time was recorded when the temperature of thermocouples was within

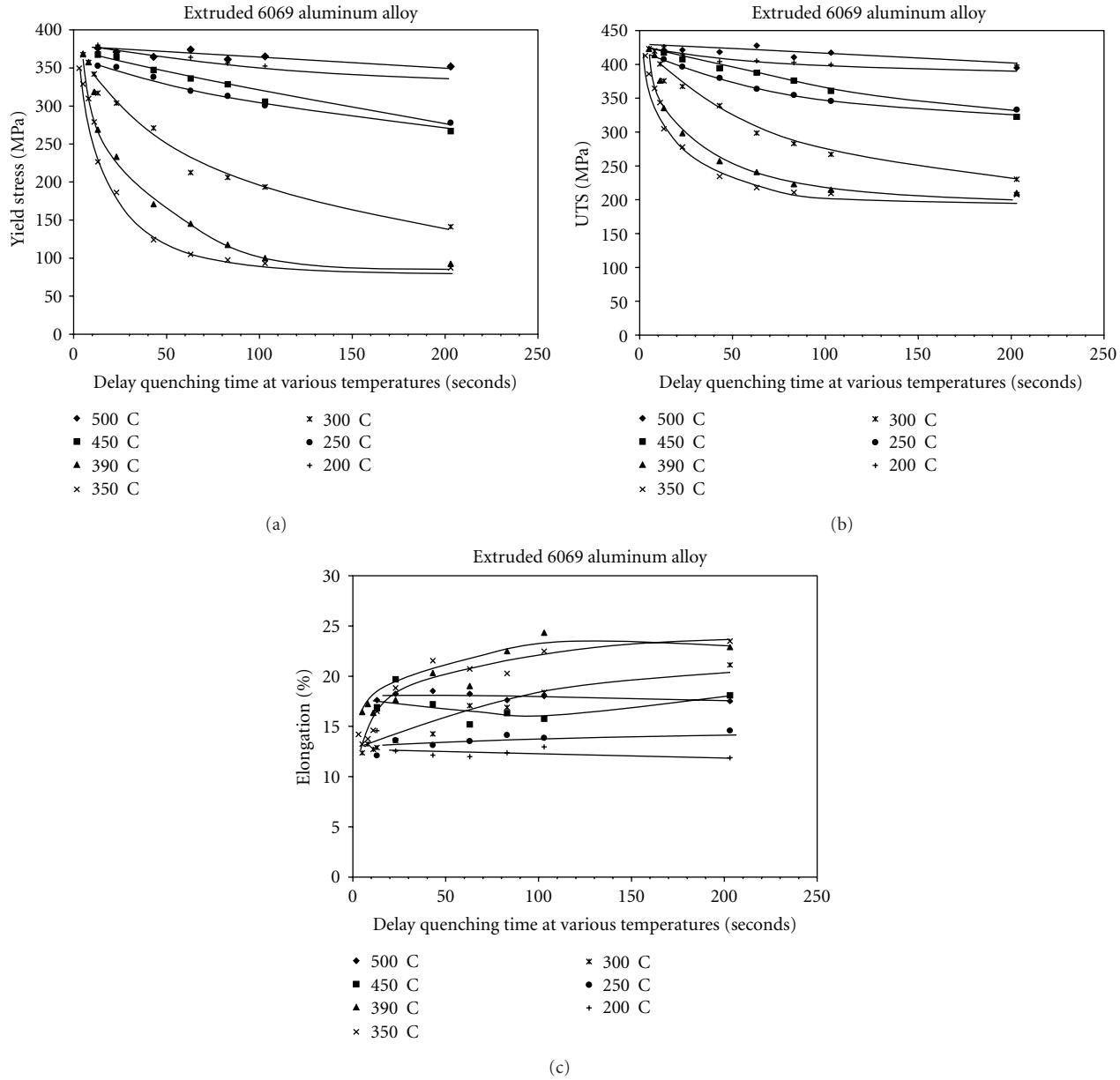

Figure 2: The effect of delayed quenching on the 6069-T6 (a) yield strength, (b) UTS, and (c) elongation.

3°C of molten salt. The precipitation (T-6) treatment for extruded 6061 and 6069 specimens was 185°C for 8 hours.

3. Results and Discussion

Figures 1 and 2 show the relationship between mechanical properties (yield stress, UTS, and elongation) of the extruded 6061-T6 and 6069-T6 alloys and the delay quenching time at various (isothermal) temperatures (200–500°C). It was found that the (0.2% offset) yield stress and UTS of both alloys decreased as the hold time increased at a given isothermal temperature. It was also observed that, at a given hold time, the strength of both alloys decreased as isothermal temperature decreased (from 500 to 350°C) and then increased again (from 200 to 300°C). The largest decreases in strength (yield and UTS) are observed at isothermal temperatures of 350–390°C for extruded 6061 and 6069. It was also observed that elongation (%) slightly increased as the hold time increased, especially at isothermal temperatures of 300–390°C.

Based on these results, the time-temperature curves at 95% of maximum (small decrease in mechanical behavior) yield stress and UTS for extruded 6061-T6 and 6069-T6 aluminum alloys are illustrated in Figure 3. The data of 95% of maximum strength were sometimes interpolated from the strength data. It is observed that extruded 6061 allows more time for a decrease to 95% of maximum strength than extruded 6069 at a given isothermal temperature. This

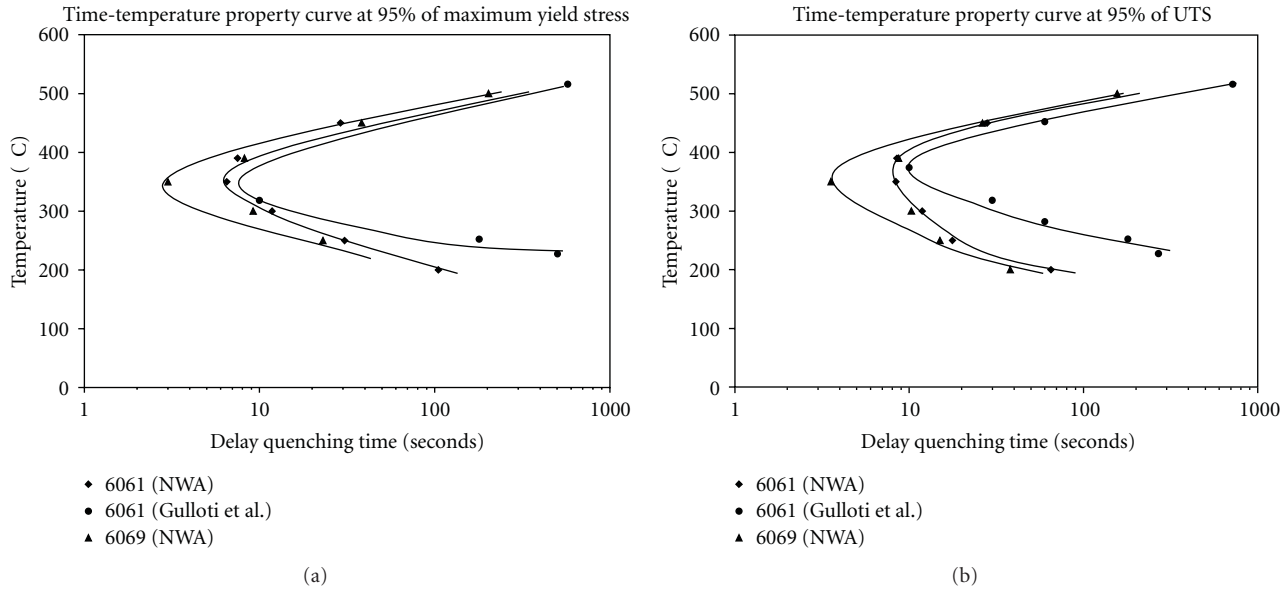

Figure 3: The time-temperature (a) yield, (b) UTS behavior of 6061-T6 and 6069-T6. Earlier work [4] on the 6061-T6 is also indicated.

indicates that mechanical properties of extruded 6069 are more sensitive to quench rate than those of extruded 6061. This is consistent with the higher levels of Mg, Si, Cu, and Cr reported in Table 1. The figure also reports other data for 6061 [4, 5]. The increased amount of magnesium, silicon and chromium may increase Mg_2Si concentration and nucleation rate, which is consistent with other studies [4]. The discrepancy between the 6061-T6 of this and the earlier study by Gullotti et al. [4], particularly at low temperatures, is not fully understood. It is curious that the 6061 of the present study shows more quench sensitivity, since the Cr, Mg, Mn, Si are all (slightly) *lower*, than that of the Gullotti study. However, a study by Camero et al. [8] of alloy 6063 shows that vanadium accelerates the precipitation kinetics of the β' and β' phases. The absences of V in [4] may explain this discrepancy. Additionally, the ratio of Mg to Si was 1.34 in this study and 1.48 in [4], with the stoichiometric ratio being Mg/Si = 2 as the β precipitates are Mg_2Si. The resulting greater excess of Si in the current study may be favorable to the formation of β' phases due to the presence of heterogeneous nucleation sites [9, 10]. Thus the increased quench sensitivity of this study, may be explained by the higher level of excess Si and the presence of vanadium. It should also be noted that the solution treatment temperature used in the present study for 6061 was 37°C higher than the standard suggested temperature, resulting in higher initial properties.

4. Conclusions

(1) 6061 and 6069 extruded aluminum alloys were solution-treated and quenched to various temperatures in salt baths between 200 and 500°C for various times, followed by water quenching. The strength of extruded 6061-T6 and 6069-T6 alloys decreased as isothermal temperature decreased from 500–350°C and then increased again from 300–200°C for fixed times at temperature. The largest strength (yield and UTS) decreases occurred at isothermal temperature of 390°C and 350°C for extruded 6061-T6 and 6069-T6, respectively.

(2) Time-temperature curves at 95% of maximum yield stress and UTS for extruded 6061-T6 and 6069-T6 aluminum alloys indicate that mechanical properties of the new alloy 6069 are more sensitive to quench rate than those of the traditional alloy, 6061.

(3) The increased quenched sensitivity appears to be due to increased amount of magnesium, silicon, and chromium (and possibly Cu), which may increase the Mg_2Si concentration and nucleation rate.

Acknowledgment

This work was partially funded through the Northwest Aluminum Company, The Dalles, Ore, USA.

References

[1] S. C. Bergsma, M. E. Kassner, X. Li, and M. A. Wall, "Strengthening in the new aluminum alloy AA 6069," *Materials Science and Engineering A*, vol. 254, pp. 161–171, 1998.

[2] F. J. MacMaster, K. S. Chan, S. C. Bergsma, and M. E. Kassner, "Aluminum alloy 6069 part II: fracture toughness of 6061-T6 and 6069-T6," *Materials Science and Engineering A*, vol. 289, no. 1-2, pp. 54–59, 2000.

[3] X. Li, M. E. Kassner, and S. C. Bergsma, "Recrystallization behavior of rolled ingots of 6061 and 6069 aluminum alloys," *Journal of Materials Engineering and Performance*, vol. 9, pp. 416–423, 2000.

[4] D. V. Gullotti, J. Crane, and W. C. Setzer, "Isothermal transformation characteristics of several 6XXX series alloys," in *Proceedings of 2nd International Aluminum Extrusion Technology Seminar*, p. 249, Atlanta, Ga, USA, 1977.

[5] H. Zoller and A. Ried, "Metallurgical aspects in development of AL MG SI alloys with a low sensitivity to quenching," *Z Metallkd*, vol. 62, pp. 354–358, 1971.

[6] S. C. Bergsma, M. E. Kassner, X. Li, and R. S. Rosen, "The Quench Sensitivity of Hot Extruded 6061-T6 and 6069-T6 Aluminum Alloys," in *Proceedings of THERMEC International Conference on Processing and Manufacturing of Advanced Materials*, T. Chandra, K. Higashi, C. Suryanarayana, and C. Tome, Eds., CD Proceedings, Las Vegas, Nev, USA, December 2000, Session A4.

[7] L. F. Mondolfo, *Aluminum Alloys: Structure and Properties*, Butterworths, London, UK, 1976.

[8] S. Camero, E. S. Puchi, and G. Gonzalez, "Effect of 0.1% vanadium addition on precipitation behavior and mechanical properties of Al-6063 commercial alloy," *Journal of Materials Science*, vol. 41, no. 22, pp. 7361–7373, 2006.

[9] K. Matsuda, Y. Sakaguchi, Y. Miyata et al., "Precipitation sequence of various kinds of metastable phases in Al-1.0mass% Mg2Si-0.4mass% Si alloy," *Journal of Materials Science*, vol. 35, no. 1, pp. 179–189, 2000.

[10] M. Muruyana and K. Hono, "Pre-precipitate clusters and precipitation processes in Al-Mg-Si alloys," *Acta Materialia*, vol. 47, pp. 1537–1548, 1999.